Research Square

Preprints are preliminary reports that have not undergone peer review.
They should not be considered conclusive, used to inform clinical practice,
or referenced by the media as validated information.

Hierarchical action of nuclear and cell surface auxin signalling in leaf-derived regeneration

Nada Kassem

Nada.Mohamed@ist.ac.at

Institute of Science and Technology Austria (ISTA) https://orcid.org/0000-0002-6448-9365

Article

Keywords: Leaf-derived regeneration.; Auxin signalling; TIR1/AFB; ABP1-TMK, cAMP; de novo root regeneration (DNRR); Wound-induced callus formation (WICF); Arabidopsis; wounding

Posted Date: November 26th, 2026

DOI: https://doi.org/10.21203/rs.3.rs-10897115/v1

License: This work is licensed under a Creative Commons Attribution 4.0 International License.
Read Full License

Additional Declarations: There is **NO** Competing Interest.

Hierarchical action of nuclear and cell surface auxin signalling in leaf-derived regeneration

Nada Kassem[1], Jiří Friml[1*]

Affiliations:

[1]Institute of Science and Technology Austria (ISTA), 3400 Klosterneuburg, Austria

ORCID IDs: 0000-0002-6448-9365 (N.K); 0000-0002-8302-7596 (J.F)

***Corresponding author.** Email: jiri.friml@ist.ac.at

Abstract

Plants have remarkable capacity to heal themselves and to regenerate organs after injury. Auxin is the main signal for regeneration but how auxin signalling coordinates this process remains unclear. Here, using leaf-derived *de novo* root regeneration and wound-induced callus formation in *Arabidopsis thaliana*, we uncover a hierarchical action of nuclear and cell surface auxin signalling mechanisms. We show that TIR1/AFB-dependent nuclear auxin signalling and downstream local cAMP production are essential for regeneration and act upstream of PIN-mediated auxin transport. Wounding induces PIN expression in the leaf aiding auxin supply to the regeneration site, whereas inhibition of TIR1/AFB signalling disrupts both processes. Exogenous auxin restores this auxin accumulation and regeneration even in the absence of TIR1/AFB activity, bypassing its requirement. We further show that ABP1/ABL-TMK cell surface auxin signalling is activated rapidly at the wound and functions locally downstream of TIR1/AFB-mediated auxin accumulation there. Disruption of the ABP1/ABL-TMK pathway compromises auxin-induced regeneration when nuclear signalling is compromised. Together, our findings establish a hierarchical mechanistic model in which nuclear auxin signalling primarily promotes PIN transcription in response to wounding enabling auxin supply to the wound site, where nuclear and cell surface signalling converge locally to execute regeneration. This hierarchical action of and cell surface signalling mechanisms in leaf derived regeneration provides an illustration to a long-standing question about how distinct auxin signalling pathways integrate in a single developmental process.

Keywords: *Leaf-derived regeneration.*; *Auxin signalling*; *TIR1/AFB*; *ABP1-TMK*, *cAMP*; *de novo root regeneration (DNRR)*; *Wound-induced callus formation (WICF)*; *Arabidopsis*; *wounding*

INTRODUCTION

Plants, as multicellular eukaryotic organisms, possess remarkable capacities for self-organization and developmental plasticity, enabling them to generate robust yet flexible patterns of growth and development under both optimal and adverse environmental conditions. These properties are exemplified by the flexible initiation and patterning of organs, the self-organized establishment of vascular networks and leaf venation, and the extraordinary capacity for tissue and organ regeneration (Ikeuchi *et al.*, 2016; Lavania *et al.*, 2021; Kong *et al.*, 2025). Auxin, a key plant hormone, plays a central role in regulating these diverse developmental processes (Friml, 2022).

Auxin signalling operates through two distinct branches: a non-canonical pathway initiated at the cell surface, and a nuclear, canonical pathway mediating transcriptional regulation (Vanneste et al., 2025; Chu et al., 2026). The cell surface signalling is mediated by the ABP1/ABL (Auxin Binding Protein 1/ABP1-like) -TMK (Transmembrane Kinase) perception module, which mediates rapid cellular effects such as ultrafast protein phosphorylation and cytoplasmic streaming (Friml et al., 2022; Yu et al., 2023; Kuhn et al., 2024) but also regulation of transcription (Cao *et al.*, 2019). On the other hand, the predominantly nuclear canonical pathway relies on TIR1 (Transport Inhibitor Response 1)/AFB (Auxin Signaling F-Box) receptors, Aux/IAA (Auxin/Indole-3-Acetic Acid) repressors, and ARF (Auxin Response Factor) transcription factors to modulate transcriptional reprogramming (Lavy & Estelle, 2016; Prigge et al., 2020; Qi et al., 2022; Chen et al., 2025). Although both pathways are essential for proper growth and development in land plants including regeneration (Mazur et al., 2020; Friml et al., 2022)**,** their relative contributions to self-organized development remain unresolved.

One of the defining features that distinguishes auxin from other plant hormones is its capacity for directional cell-to-cell transport, mediated by specialized plasma membrane-localized transport proteins. This polar transport system is primarily facilitated by the PIN-FORMED (PIN) family of auxin efflux carriers (Luschnig & Friml, 2024). Notably, following auxin perception, PIN auxin transporters undergo repolarization to specific domains of the plasma membrane, a process mediated by phosphorylation through various kinases and regulatory proteins. This cellular repolarization enables flexible redirection of auxin transport within tissues, thereby contributing to self-organized development (Sauer *et al.*, 2006; Zhang *et al.*, 2020). Both canonical and non-canonical auxin signalling pathways contribute to PIN polarization.

The nuclear pathway mediate expression of the transcription factor WRKY23 and its downstream targets, receptor-like kinases CAMEL (Canalization-related Auxin-regulated Malectin-type RLK) and CANAR (Canalization-related Receptor-like kinase), which regulate auxin-induced PIN phosphorylation and localization required for regeneration (Hajný et al., 2020) The cell surface ABP1-TMK1 signalling also promotes PIN polarization through direct interaction and phosphorylation (Rodriguez *et al.*, 2025; Huang *et al.*, 2026) This feed-back regulation of auxin transport by the converging action of both auxin signalling pathways is central to so called “auxin canalization”, a flexible, self-organizing mechanism that guides long-distance auxin flow from the source to the sink, leading to tissue patterning, organogenesis and regeneration (Sachs, 2000; Ravichandran et al., 2020; Aliaga Fandino & Hardtke, 2022; Hajný et al., 2022).

Plants as sessile organisms rely on robust adaptive mechanisms to survive environmental and mechanical stresses. One of the most striking of these adaptations is their ability to regenerate tissues after injury. Following wounding, differentiated cells can re-enter developmental programs that enable the formation of new organs (Sugimoto *et al.*, 2011; Duclercq *et al.*, 2011; Xu & Huang, 2014; Kareem *et al.*, 2025). Two prominent examples are *de novo* root regeneration (DNRR) and wound-induced callus formation (WICF), in which adventitious roots or calli arise from wounded leaf petioles depending on water availability (Kareem *et al.*, 2025). DNRR or WICF can be induced in tissue culture by supplementing media with auxin (Ikeuchi *et al.*, 2026). The same tissue can also regenerate on hormone-free medium, relying solely on endogenous auxin, although root or callus formation typically occurs more slowly (Birnbaum & Alvarado, 2008; Xu & Huang, 2014; Chen *et al.*, 2014; Kareem *et al.*, 2025). In DNRR, which is composed of four steps, each step is controlled by specific transcription factors. During endogenous callus formation (first step), the transcription factors WIND1 (WOUND-INDUCED DEDIFFERENTIATION 1) and WOX11 (WUSCHEL-RELATED HOMEOBOX 11) play central roles. In the second step, callus specialization into root founder cells is mediated by WOX11 together with WOX12. For root primordium formation (third step), WOX5 and WOX7 are upregulated; downstream of WOX11 and WOX12. Then in the last, fourth step, these coordinated transcriptional events culminate in root emergence from the developing primordium (Fan *et al.*, 2012; Bustillo-Avendaño *et al.*, 2018). In the case of WICF, it is believed that other transcription factors mediate callus formation, such as LBD16 (LATERAL ORGAN BOUNDARIES DOMAIN 16) and LBD29 (Bustillo-Avendaño *et al.*, 2018; Kareem *et al.*, 2025). Nonetheless, despite these insights into downstream processes culminating in regeneration, how auxin and its both signalling mechanisms initiate the whole process remain unclear, representing a conceptual gap in understanding regeneration and self-organized development.

Here, using excised Arabidopsis leaf petioles, we investigate how nuclear and cell surface auxin signalling pathways converge on root and callus formation establishing the hierarchical organization of both auxin signalling pathways upstream of leaf-derived regeneration.

RESULTS

Optimization of *de novo* root regeneration and wound-induced callus formation assays

To investigate a potential role of auxin signalling and transport in leaf-derived regeneration, we first optimized previously described protocols for DNRR and WICF from detached leaves (Chen *et al.*, 2014; Kareem *et al.*, 2025). Establishing robust assay conditions was critical to enable systematic testing of mutants across multiple regulatory pathways. We evaluated key experimental parameters, including medium composition, light conditions, and the timing of leaf petiole excision, which significantly influenced the regenerative outcome to identify the optimal conditions that supported quantifiable and consistent responses (Fig. S1a)

A recent study (Kareem et al., 2025) showed that local water availability at the wound site plays a decisive role in shaping the regeneration outcomes – whether root or callus is formed. To further elucidate the impact of water availability on regenerative outcomes, we tested different concentrations of agar. Under touch conditions (0.75% agar), trimmed petioles regenerated roots, whereas under non-touch conditions (3% agar or flipped explant to face the plate lid), callus formation was predominant (Fig. 1a). We used also the intermediate medium (1.5%; explants touch the medium), which shows all: calli, roots, and roots regenerating after one- or two-days following callus formation (Fig. 1b). After testing several agar concentrations (1.5%, 2%, 2.5%, 3%) and effect of auxin transport inhibitor 1-N-naphthylphthalamic acid (NPA) as a test compound, the 1.5% medium was found best suited for testing effects of chemical treatments as it can combine drought stress while still allowing absorbing substrates from the medium (Fig. S1b).

Concerning light and sucrose supplementation, the most reliable and consistent outcomes were observed under dark conditions with sucrose-enriched medium. A detailed protocol allowing for robust and consistent outcomes can be found in the materials and methods section.

PIN-dependent auxin transport and PIN trafficking in leaf-derived regeneration

Using the optimized conditions, we first tested the importance of PIN-dependent polar auxin transport for leaf-derived regeneration across both high and low water availability scenarios by using 1.5% intermediate medium. We employed NPA, an established auxin transport inhibitor, which directly targets PIN auxin transporters (Tan, 2021). Supplementing 1.5% medium with NPA (1 µM, 2 µM) revealed a concentration-dependent inhibition of regeneration in the wild type (Col-0), affecting both root and callus formation (Fig. S2a). We complemented this pharmacological approach by testing the segregating *pin1+/-* mutant population under touch (0.75%) and non-touch conditions (Fig. S2b,c). Previous reports (Kareem., et al, 2025) shows that *pin3;4;7*

mutants do not show much defects in DNRR and WICF, likely due to the high redundancy while *pin1* shows defect in both touch and non-touch conditions (Fig. S2b,c), consistent with our data. This shows that PIN-dependent auxin transport is involved in both DNRR and WICF.

To gain additional insights into the role of PIN auxin transporters in leaf-derived regeneration, we performed a time course of PIN3, PIN4, and PIN7 expression in DNRR and WICF using *pPIN:GUS* lines. In response to wounding, the activity of *PIN3*, *PIN4*, and *PIN7* promoters was strongly induced n the main vein and in the proliferative area above the wound (in case of DNRR) or close to the wound site (for WICF) (Fig. S2d,e). This suggests PIN involvement in both, long-distance auxin delivery from the leaf blade and at all stages of root and callus regeneration itself. For PIN1, we tested *pPIN1:PIN1-GFP* line under both touch and non-touch conditions, and it shows strong expression at proliferative cells (during DNRR) and close to the wound site (during WICF), supporting the idea that PIN1 is required in this area for root as well as callus formation (Fig. S2f,g). Overall, these findings support a role of long-distance auxin transport through different PINs in mediating both, DNRR and WICF, and the possible redundancy between different PINs, as suggested by overlapping expression patterns and only partial defects in different *pin* mutants as compared to full NPA-based auxin transport inhibition.

Next, we investigated importance of PIN trafficking in leaf-derived regeneration, using both, pharmacological and genetic interference. We used the 1.5% intermediate medium supplemented with 10 µM Brefeldin A (BFA), which targets ARF GEF (ADP-Ribosylation Factor Guanine Nucleotide Exchange Factor) trafficking regulators, chiefly GNOM, to inhibit PIN recycling to the plasma membrane leading to intracellular PIN accumulation in so called BFA bodies (Adamowski *et al.*, 2024) tested BFA effect on DNRR, WICF, and calli with roots (WICF+DNRR). We observed a significant, concentration-dependent effect on regeneration efficiency manifested by an almost complete inhibition in DNRR, WICF, and WICF+DNRR (Fig. 1c). Analysis of the weak *gnom* R5 allele also showed consistent defects in both, DNRR in touch (Fig. 1d) and WICF in non-touch conditions (Fig. 1e). In addition to decreased regeneration efficiency, smaller calli (< 50% of the Col-0 calli) were detected in non-touch conditions in *gnom* R5 (Fig. 1f).

Overall, these findings strongly support the role of BFA-sensitive, ARF GEF-dependent PIN trafficking in mediating leaf-derived root and callus regeneration.

TIR1/AFB-mediated nuclear auxin signalling in leaf-derived regeneration

After establishing the role of PIN-mediated auxin transport in leaf-derived regeneration, we next tested role of the transcriptional auxin pathway mediated by TIR1/AFB nuclear receptors (Vanneste et al., 2025; Chu et al., 2026). First, we examined DNRR under touch conditions (0.75% agar) in *tir1* and *tir1;afb2;afb3* mutants defective in the nuclear

auxin perception. The *tir1* mutant showed a noticeable decrease in DNRR, but the defect was dramatically amplified in *tir1;afb2;afb3*, which exhibited a striking 98% failure rate as early as day 7 till the end of the experiment (day 15) (Fig 2a,b). Next, we investigated the WICF under non-touch conditions. The *tir1;afb2;afb3* exhibited a significant reduction in WICF as early as day 7, compared to both, Col-0 and *tir1*, which maintained robust callus regeneration capacity (Fig 2c). Further analysis of callus size revealed that both, *tir1* and *tir1;afb2;afb3* produced smaller calli as compared to Col-0, with *tir1;afb2;afb3* being the smallest (Fig 2d,e). To test importance of transcriptional regulation downstream of TIR1/AFB receptors, we conditionally expressed the gain-of-function *axr3/iaa17* transcriptional repressor using the XVE*>>axr3-mCherry* estradiol inducible system, which was shown to inhibit auxin-mediated processes (Chen *et al*., 2025). Induction of *axr3-mCherry* expression caused a strong inhibition of both DNRR and WICF on the 1.5% intermediate medium with defects becoming evident by day 7 as compared to the non-induced control (Fig 2f). These observations revealed a redundant role of TIR1/AFB auxin receptors and downstream transcriptional signalling in both, DNRR and WICF processes during leaf-derived regeneration.

Building on recent work on cAMP (cyclic Adenosine Monophosphate) production by TIR1/AFB receptors and their role in transcriptional auxin signalling (Qi et al., 2022; Chen et al., 2025), we examined whether localized production of cAMP is involved in leaf-derived regeneration. We used the *XVE>>axr3-mCherry-KUP5* line, to inducibly express *axr3-KUP5* (Auxin Resistant 3 - K^+ Uptake Permease 5), which generates cAMP locally in the context of TIR1/AFB-Aux/IAA-ARF signalling (Chen *et al*., 2025). The *axr3-KUP5* induction on 1.5% intermediate medium completely rescued the regeneration defects of *axr3* in both DNRR and WICF assays, whereas the expression of mutated *axr3-KUP5m* version with compromised cAMP production failed to rescue, showing no regeneration, progressive chlorophyll loss, and eventual tissue collapse (Fig. 2g, h, i). Two independent lines for both, *XVE>>axr3-mCherry-KUP5* and *XVE>>axr3-mCherry-KUP5m* were tested in this context, showing similar effects.

We also tested the exogenous application of the membrane-permeable 8-Br-cAMP to leaf explants under touch conditions (0.75% agar; 35 µM or 200 µM). Treatment with 35 µM cAMP did not visibly affect timing of root formation, but consistently produced longer regenerated roots compared to untreated controls, indicating enhanced DNRR efficiency and a faster progression of root outgrowth (Fig. 2j, k). In contrast, the high concentration (200 µM) produced outcomes comparable to untreated Col-0 explants, indicating that increasing cAMP beyond the optimal range does not confer additional benefit (data not shown). Together, these observations suggest that cAMP promotes regeneration only within a narrow concentration window: modest elevation enhances root formation and elongation, whereas higher levels are not effective.

Together, these results demonstrate that TIR1/AFB auxin receptors and downstream signalling including cAMP production are essential for leaf-derived regeneration.

Exogenous auxin rescues the TIR1/AFB deficiency in leaf-derived regeneration

Next, we wondered whether the strong permanent defects in leaf-derived regeneration observed in *tir1;afb2;afb3* mutant are caused by primarily by defect in auxin perception at the site of regeneration. Therefore, we supplemented the medium for touch conditions with the stable, synthetic auxin 1-Naphthaleneacetic acid (NAA). Notably, treating *tir1;afb2;afb3* explants with NAA (0.2 µM and 2 µM NAA) rescued its regeneration defect (Fig. 3a). Low auxin concentrations (0.2 µM) partially rescued it through direct DNRR forming shorter roots with lack of root hairs as compared to Col-0 (Fig. 3b,c,d), while the high auxin (2 µM) completely rescued it through indirect DNRR (first induction of callus formation with root formation as a second response) (Fig. 3a).

The obvious rescue of *tir1;afb2;afb3* regeneration defects by exogenous auxin raised a question about which auxin receptor(s) mediate this effect in the absence of TIR1/AFB2/AFB3? Candidates include the remaining members of the TIR1/AFB family or the alternative auxin perception mechanism at the cell surface mediated by the ABP1-TMK module (Friml et al., 2022). To address this, we used Auxinole, which can bind and block all 6 receptors from the TIR1/AFB family (Hayashi *et al.*, 2012). As expected Auxinole (50 µM) inhibited leaf-derived regeneration on intermediate (1.5%) medium confirming that it is effective (Fig. 3e). Next, we tested whether in presence of Auxinole (50 µM), NAA (0.2 µM and 2 µM) can still rescue the DNRR in Col-0 or *tir1;afb2;afb3*. Surprisingly, both genotypes still showed robust regeneration rescue under these conditions with *tir1;afb2;afb3* rescued only under high NAA conc (2 µM) in the presence of Auxinole (Fig. 3f,g,h). This strongly suggests that the receptor(s) involved in this effect are outside the canonical TIR1/AFB family.

Overall, these observations show that a deficiency in the nuclear TIR1/AFB pathway can be rescued by the exogenous auxin application, suggesting involvement of additional auxin perception mechanisms.

ABP1/ABL-TMK cell surface auxin perception in leaf-derived regeneration

The prime auxin perception candidate that may mediate the NAA-dependent rescue in the absence of the nuclear auxin receptors functionality, is the cell surface auxin signalling pathway involving ABP1 and TMKs. To evaluate its potential role in leaf-derived *de novo* root regeneration, we focused on the core components of this pathway, ABP1 receptor and its structural homologs ABL1, ABL2 and ABL3 and the TMK co-receptor family (Friml et al., 2022; Yu et al., 2023; Rodriguez et al., 2025).

First, we examined the expression patterns of ABP1, ABL3, TMK1, TMK3, and TMK4 using *promotor:GUS* lines. The *pABP1:GUS* showed strong increase in promoter activity both at the wound site (proliferative cells plus the neighbouring cells) and across the leaf blade as early as 3 hours after cutting (3 HAC), which was not observed prior dissection (Fig 4a1). Under non-touch conditions, the signal was strong in the callus

area and the leaf blade in response to cutting (Fig. 4c1); suggesting that ABP1 is rapidly engaged during both DNRR and WICF. Next, we examined the *pABL3:GUS* line in both touch and non-touch conditions. ABL3 exhibited detectable promoter activity at the wound site from the first day after cutting. Although the initial signal was weaker than that of ABP1, ABL3 expression increased dramatically during regeneration progression, ultimately surpassing ABP1 signal intensity (Fig. 4a2 and 4c2). This temporal pattern supports the redundant action of ABP1 and ABLs (as exemplified here by ABL3) during leaf-derived regeneration.

pTMK1:GUS reporter displayed strong promoter activity throughout the leaf explant, including the main vein and the wound site during both DNRR and WICF. Notably, this intense TMK1 signal appeared rapidly within 3–4 hours after cutting the leaf petiole and was completely absent in intact leaves prior to detachment (Fig. 4a3 and 4c3). This early wound-induced activation of TMK1 expression closely mirrors that of ABP1, suggesting that TMK1 is also engaged at the very initial stages of DNRR and WICF. Interestingly, signals for all ABP1, ABL3, and TMK1 appeared very rapidly on the first day after cutting and they remained strong till the leaf petiole emerged roots/calli from the wound. Next, we examined the *pTMK3:GUS* and *pTMK4:GUS* reporter lines. Both, TMK3 and TMK4 showed promoter activity at the wound site, particularly in the proliferative vascular cells (Fig. 4a4,5 and 4c4,5). Although neither reporter displayed a detectable signal immediately after cutting, both were strongly induced by 2 or 3 days after detachment (Fig. S3e1,2). Their expression persisted throughout the subsequent stages of the regeneration during both DNRR and WICF. The overlapping expression patterns of TMK1, TMK3 and TMK4 indicate that they all may participate redundantly in the root and callus regeneration processes.

We also analysed *pTMK1:TMK1-GFP* and *pTMK4:TMK4-GFP* translational fusion lines by confocal microscopy during DNRR to visualize the protein themselves. At 1 DAC, TMK1 and TMK4 showed strong expression in the proliferative cells area. From 3 or 4 DAC onward, TMK4 accumulated robustly around the wound area and localized to the plasma membrane of wound-adjacent cells, with signal intensity increasing over time (Fig. 4b and S3d). During root primordium formation and root emergence (6 and 8 DAC), TMK4-GFP remained strongly enriched at the plasma membrane of the developing primordium and the emerging roots, an expression pattern not observed for the TMK1 (Fig. 4b and S3d). These observations indicate that TMK4 acts as the dominant and sustained cell surface auxin receptor during DNRR. In addition, TMK1-GFP also showed a strong expression during WICF (Fig. 4d).

Next, we tested the phenotypes of mutants defective in ABP1/ABL-TMK auxin perception. None of the tested mutants including *abp1;abl1;abl2*, *tmk1;2;3*, or the corresponding single mutants displayed consistent defects in DNRR or WICF compared to Col-0. Regeneration outcomes, specifically with these genotypes were very variable; only *tmk4* mutant showed consistently defect in root regeneration, and in callus size but not in callus formation as compared to Col-0 (Fig. S3a, b, c). A more definitive test of

the involvement of the cell surface auxin signalling pathway is limited by several factors: the lack of a specific inhibitor and *in vivo* reporter for the cell surface signalling and the limited viability and fertility of the *tmk1;2;3;4* quadruple mutant.

Next, we tested the role of these components under conditions of inhibited TIR1/AFB nuclear auxin signalling. We used the 1.5% intermediate medium and treated *tmk1;2;3* explants with 50 µM Auxinole and 2 µM NAA. This strategy allowed us to completely block nuclear auxin signalling and all TMK-dependent cell surface signalling except TMK4 (Fig. 4e). Under these conditions, the leaf-derived regeneration in *tmk1;2;3* was not efficiently rescued by NAA in contrast to Col-0 controls (Fig. 4f,g).

Overall, these observations show that multiple ABP1/ABL and TMK components of cell surface auxin perception are upregulated and expressed in overlapping patterns during leaf-derived regeneration and they are essential for exogenous auxin-induced rescue of DNRR and WICF in absence of functional nuclear auxin signalling.

TIR1/AFB- and PIN-mediated auxin delivery to regeneration site

Next, we tried to understand what are the distinct roles of nuclear TIR1/AFB and cell surface ABP1/ABL-TMK auxin perception mechanisms in the leaf-derived regeneration. The observation that loss of nuclear auxin signalling can be rescued by exogenous auxin supply (see Fig. 3h) suggests that this pathway may be involved in delivery of auxin to the regeneration site.

To test this hypothesis, we chemically blocked PIN-dependent auxin transport and resupplied exogenous auxin using a touch medium (0.75%) containing 2 µM NPA + 0.2 µM NAA or 2 µM NAA (Fig. 5a). As seen for inhibition of TIR1/AFB signalling by Auxinole (Fig. 3h), also in this case, exogenous NAA restored regeneration competence in the presence of NPA supporting the scenario that TIR1/AFB signalling is required for the auxin delivery to the wound site.

To further test this notion, we visualized asymmetric auxin distribution during leaf-derived regeneration using a synthetic auxin-response reporter DR5. As compared to previous reports (Bustillo-Avendaño *et al.*, 2018; Kareem *et al.*, 2025), we performed a more detailed time course analysis using confocal microscopy to reveal the auxin response distribution during different stages of DNRR and WICF. DR5 signal before cutting is low in the main vein and the base of the leaf. After excision, during DNRR, DR5 gets rapidly increased across the main vein, and the whole base of the cut leaf and at later time points it gets restricted to the proliferative cells area above the wound site. By day 4-5, the signal is high in forming root primordia and at later in the emerging root (day 6-7) (Fig. 5b). During WICF, DR5 signal gets also upregulated in the main vein, however, rather at the wound site itself and gradually increases till the formation of the callus at the base of the wound while, the callus itself has no DR5 signal (Fig. 5c).

The same analysis during DNRR under conditions of inhibited auxin transport (NPA; 0.75%) revealed strong depletion of DR5 signal at the regeneration site and its re-appearance following exogenous auxin treatment (NPA+NAA; 0.75%) (Fig. 5d and S5a). This confirms that inhibition of PIN-dependent auxin transport prevents auxin delivery to the regeneration site, which can be resupplied by exogenous auxin treatment (Fig. 5e).

Unfortunately, use of the DR5 reporter depends on the nuclear auxin signalling preventing us from performing similar experiments with Auxinole. Nonetheless, the observations that interference with both, auxin transport (NPA) or TIR1/AFB auxin signalling (mutants, Auxinole), block leaf-derived regeneration that can be in both cases rescued by exogenous auxin resupply (Fig. 5a and 3h) together with an apparent auxin depletion at the wound site following inhibition of auxin transport by NPA and its resupply by exogenous auxin treatment (Fig. 5d,e); all support a role of nuclear auxin signalling in supplying auxin to the regeneration site.

Overall, these observations suggest that TIR1/AFB signalling pathway is primarily involved in auxin supply to the wound site.

TIR1/AFB auxin signalling controls PIN expression to support auxin supply and enable downstream ABP1/ABL-TMK signalling at the regeneration site

Next, we addressed a mechanism, by which TIR1/AFB nuclear auxin signalling mediates auxin delivery to the regeneration site. We blocked TIR1/AFB signalling by Auxinole on intermediate (1.5%) medium and examined expression of PIN auxin transporters using *pPIN:GUS* lines. GUS staining of *pPIN3:GUS*, *pPIN4:GUS*, and *pPIN7:GUS* showed that treatment with 50 µM Auxinole completely suppresses PIN expression (Fig. 6a), which normally gets upregulated after wounding (see Fig. S2d,e). This explains the disrupted long-distance auxin transport from the leaf blade to the wound leading to regeneration failure observed in conditions of inhibited TIR1/AFB signalling (see Fig. 2).

To determine how exogenous NAA is locally redirected within the wound region, we again analysed *pPIN3/pPIN4/pPIN7:GUS* lines, this time under 2 µM NPA + 0.2 µM or 2 µM NAA co-treatment (0.75%). NAA rapidly re-induced PIN expression despite the presence of NPA (Fig. 6b, Fig. S4a,b,c and Fig. 6c) confirming auxin-induced regulation of PIN expression in this context.

These observations indicate that regeneration competence requires the local convergence of the two auxin signalling pathways: (i) nuclear auxin signalling, which primarily drives PIN-dependent long-distance auxin supply to the wound site from the tissues above but also provides the transcriptional reprogramming capacity for regeneration; and (ii) ABP1–TMK cell surface signalling, which operates locally to execute the regeneration program. In this view, cell surface auxin signalling acts

downstream of auxin nuclear signalling and is fully dependent on activity of the nuclear auxin signalling, which mediates auxin supply to regeneration site (Fig. 6d).

DISCUSSION

The two distinct auxin signalling pathways – the TIR1/AFB-mediated nuclear and the ABP1/ABL-TMK-dependent at the cell surface – have been shown to activate distinct sets of cellular processes often converging on overlapping developmental outputs. Nonetheless, how these two pathways are integrated and coordinated remain a key, long standing question in the field (Sheen, 2024). Here, on example of organ regeneration in the excised leaf, we identified a hierarchical, spatially separated action of these pathways with TIR1/AFB pathway enabling long-distance auxin delivery to the wound site, where local convergent action of both, TIR1/AFB and ABP1/ABL-TMK signalling mechanisms allows regeneration. In this scenario, TIR1/AFB pathway acts upstream of ABP1/ABL-TMK signalling; both activities being linked by the intercellular auxin transport, mediated by PIN auxin transporters.

We show that wounding (excising the leaf) leads to transcriptional upregulation of PIN auxin transporters across the leaf main vein and accumulation of auxin (as inferred from DR5 auxin response reporter) at the wound site, where regeneration occurs. When PIN-dependent auxin transport or PIN trafficking are compromised, the auxin accumulation at the wound site does not occur and regeneration does not occur.

Genetic or pharmacological inhibition of the TIR1/AFB signalling leads to near complete, permanent loss of regeneration, whereas local production of cAMP promotes regeneration. This establishes TIR1/AFB – cAMP mechanism as indispensable for regeneration. Notably, its disruption also suppresses the wound-induced upregulation of PIN auxin transporters suggesting that TIR1/AFB nuclear signalling is required to for the PIN-mediated long distance auxin transport to the wound site, where regeneration occurs. Consistent with this, a recent study (Pérez-Henríquez *et al*., 2024) reported that nuclear auxin signalling is also upstream of auxin biosynthesis. The key role of TIR1/AFB pathway to supply auxin to the regeneration site is confirmed by the ability of the exogenously supplied auxin to rescue regeneration competence even if the TIR1/AFB signalling is blocked. Nonetheless, action of the nuclear signalling is likely not confined only to the leaf blade: it remains active also at the wound site as evidenced by DR5 reporter activity showing strong local activation of auxin-induced transcription during regeneration. Thus, TIR1/AFB nuclear auxin signalling operates at two spatially-separated levels; (i) globally to induce auxin biosynthesis and establish auxin flow from the leaf blade to the regeneration site, and (ii) locally at the regeneration site to interpret auxin accumulating there to aid regeneration.

Our expression analysis also shows that cell surface ABP1/ABL-TMK signalling components are activated rapidly after wounding, with ABP1 and TMK1 strongly expressed already 3 hours after cutting and TMK1 and TMK4 accumulating at the

plasma membrane of proliferative cells during regeneration. Although redundancy within these families likely masks strong defects in mutants with exception of *tmk4*, which shows consistent defects, the sensitized conditions (inhibited nuclear signalling with auxin resupplied exogenously) exposed regeneration defects in *tmk1;2;3* mutants, revealing a role of the ABP1/ABL-TMK signalling at the regeneration site following auxin accumulation there. Under non-disturbed conditions, this action is likely masked by the parallel action of TIR1/AFB nuclear signalling and the remaining TMK4 during regeneration.

Thus, both TIR1/AFB and ABP1/ABL-TMK play key roles in regeneration. Crucially, ABP1/ABL-TMK cannot compensate for loss of TIR1/AFB signalling because of non-redundant action of TIR1/AFB pathway mediating PIN expression and auxin supply to the regeneration site. When TIR1/AFB signalling is compromised, both processes collapse, auxin does not reach the wound, and thus ABP1/ABL-TMKs lack the auxin input. Conversely, when auxin is supplied exogenously and reaches the wound site, this pathway can activate regeneration even when nuclear signalling is compromised.

Together, these observations support a unified model in which non-redundant action of nuclear auxin signalling establishes auxin biosynthesis, PIN expression, and long-distance auxin transport to the wound, while both, nuclear and cell surface signalling interpret together auxin accumulating locally there to execute regeneration. Presumably, TIR1/AFB signalling mediates the transcriptional reprogramming for cell fate acquisition during regeneration, while ABP1-TMK provides input from the cell surface, presumably refining local auxin fluxes through direct phosphorylation of PIN proteins (Rodriguez *et al.*, 2025; Huang *et al.*, 2026) and/or regulation of cell division orientation by activation of downstream MAPK pathway (Huang et al., 2019).

Auxin-induced regeneration therefore emerges not from parallelly acting auxin signalling pathways but from a spatially separated, hierarchical cascade that integrates TIR1/AFB-dependent global auxin supply from the leaf acting upstream of local signalling activation at the regeneration site involving both, TIR1/AFB and ABP1/ABL-TMK pathways.

These findings not only provide crucial insights into how auxin induces organ regeneration after wounding – a mechanistically fascinated process with extensive agriculture relevance – but also provides an example how the two known auxin signalling mechanisms are integrated and coordinated to converge on a single developmental output; something that is considered a long-standing enigma in the field (Sheen, 2024). Given that many other developmental processes (e.g. vasculature reconnection, embryogenesis, lateral root organogenesis) involve both auxin signalling pathways as well as PIN-mediated auxin transport (Vanneste *et al.*, 2025), it is well possible that variants of here identified mechanism are involved in other developmental processes beyond the organ regeneration.

Material and methods

Plant materials and growth conditions

Arabidopsis thaliana ecotype Columbia-0 (Col-0) was used as the wild type in this study. All Arabidopsis mutants and transgenic lines employed are listed in Table S1, including references. To ensure aseptic conditions for seed-based experiments, a chlorine gas sterilization protocol was applied for surface sterilization of all seeds. Briefly, seeds were placed in open microcentrifuge tubes and arranged inside a sealed container within a fume hood. Chlorine gas was generated by adding approximately 3 mL of concentrated hydrochloric acid (37%) to 100 mL of household bleach (sodium hypochlorite, ~5–6%) using a syringe pipette. Immediately after the addition, the container was tightly sealed and incubated for 24 hours to allow thorough gas exposure. Following sterilization, the seed tubes were opened and placed under laminar airflow in a sterile hood for at least 2 hours to dissipate residual chlorine gas before use. Then the sterilized seeds were sown on AM+ medium, which is half-strength Murashige and Skoog (MS) medium with 0.5% sucrose, 0.25 g/l MES buffer, pH 5.7–5.75, and 0.8% (w/v) plant agar. After 2 days of stratification at 4 °C in the dark, seedlings were grown vertically at 22 °C under a 16-hour light (110 µE intensity) and 8-hour dark photoperiod.

Constructs and Transformation

To generate *TMK4::TMK4-GFP* lines in the *tmk4-1* background, the full-length *TMK4* genomic sequence (without stop codon) was amplified from Col-0 seedling DNA by PCR and inserted into the pDONR221 entry vector via BP recombination. For assembly of the *TMK4::TMK4-GFP* construct, three entry vectors—pDONR P4-P1R containing the 2-kb *TMK4* promoter, pDONR221 containing gTMK4, and pDONR P2R-P3 containing GFP—were recombined into the pB7m34GW destination vector using MultiSite Gateway LR recombination. The final construct was transformed into *Agrobacterium tumefaciens* strain GV3101 by electroporation and subsequently introduced into Col-0 plants by floral dip.

Wounding and regeneration assays

For regeneration experiments, the first pair of true leaves with approximately 0.5 mm petioles was excised from 12-day-old *Arabidopsis* seedlings using sterile microscissors within a sterilized laminar hood. The detached leaf explants were immediately transferred onto hormone-free Gamborg B5 medium (micro and macro salts with vitamins; Duchefa Biochemie, G0210), supplemented with 100 mM sucrose, 0.5 g L^{-1} MES buffer (adjusted to pH 5.7 with NaOH), and 0.75% (w/v) plant agar. Explants were positioned either with the wound site in direct contact with the semi-solid medium 0.75% (abaxial side facing down) for touch conditions or with the wound site not touching the semi-solid medium 0.75% (adaxial side facing down) for non-touch conditions, to assess the influence of orientation on regeneration outcomes. For touch and non-touch conditions without treatment, we use 0.75% +B5 medium, while for intermediate medium, which was used for drought-treatment, we use 1.5% +B5 (w/v) plant agar.

Plates were incubated under standard growth conditions in the dark, and regeneration responses were documented at multiple time points—typically on days 7, 9, and 12 post-wounding. Each genotype was analysed using three biological replicates, with one plate per replicate. Each plate has 30 explants, so a total of 90 explants per genotype. Each experiment is repeated at least two times independently under the same conditions.

Chemical treatments

For inhibition of polar auxin transport, 1 µM or 2 µM N-1-naphthylphthalamic acid (NPA), which was dissolved in double-distilled water, was added to the +B5 medium. Trimmed leaf explants were cultured on intermediate medium 1.5% +B5. Since NPA was water-soluble in this setup, no organic solvent was required for the mock treatment, ensuring that solvent effects did not confound the regeneration response. Naphthaleneacetic acid (NAA; synthetic auxin) was dissolved in double-distilled water with the addition of 2–3 drops of NaOH to aid solubilization. For the inhibition of PIN trafficking, 1.5% Intermediate medium was supplemented with 10 µM brefeldin A (BFA; MedChemExpress, HY-16592). BFA was dissolved in ethanol, and the same volume of ethanol was added to mock-treated plates. For the inhibition of the nuclear auxin signalling pathway, 1.5% B5 intermediate medium was supplemented with 50 µM Auxinole (MedChemExpress, HY-111444). Auxinole was dissolved in ethanol with gentle warming, and the same volume of ethanol was added to mock plates. For the chemical induction of *XVE>>axr3-mCherry* lines, 1.5% +B5 Intermediate medium was supplemented with 5 µM β-estradiol. β-Estradiol–cyclodextrin complex (water-soluble β-estradiol, E4389, Sigma-Aldrich; containing 40–55 mg estradiol per g solid) was dissolved in Double distilled water and then used at a final estradiol concentration of 5 µM .

GUS staining

Samples were stained following the protocol of Yang *et al.* (2013) with minor modifications. Briefly, β-glucuronidase (GUS) reporter seedlings were cut at the leaf-petiole region from 12-day-old plants and harvested at defined time points after cutting (1, 4, and 8 or 9 days after cutting, then culturing on B5 medium; DAC). At each time point, explants were incubated in cold acetone for 20 min to enhance tissue permeability, then washed with washing buffer (0.5 mM ferrocyanide, 0.5 mM ferricyanide, 50 mM NaH_2PO_4, 50 mM Na_2HPO_4, and 1% Triton X-100; pH=7) for 10 min to remove residual acetone. Explants were subsequently submerged in GUS staining solution (washing buffer supplemented with 1 mM X-Gluc; Thermo Fisher Scientific) and placed under vacuum for 10 min to facilitate substrate infiltration. For *pPIN:GUS* lines, 4 mM X-Gluc was used while for *pABP1/TMK:GUS* lines, 1 mM conc was used. Tissues were then incubated in GUS buffer at 37 °C overnight. The reaction was stopped by washing the explants with washing buffer for 10 min in the dark. To remove chlorophyll background, explants were incubated in 70% ethanol overnight in the dark (renew ethanol 70%), followed by incubation in chloral hydrate (Sigma-Aldrich) solution for one

or two days to clear remaining chlorophyll; dark. Finally, explants were mounted on slides in chloral hydrate solution and imaged using an Olympus microscope with 4×, 10×, and 20x objective lenses.

Tissue fixation and clearing for confocal imaging

Wounded leaf explants carrying different fluorophores were fixed, cleared, and stained for cell-wall visualization before confocal imaging, using a protocol adapted from Kareem et al. (2025). Tissues were fixed in 4% paraformaldehyde in 1× PBS containing 0.1% Triton X-100 for 1 h at room temperature, including a 10-min vacuum step. After fixation, samples were washed twice in 1× PBS; 5 mins each and sequentially incubated in absolute methanol and absolute ethanol for 30 min each. Following an additional PBS wash, tissues were cleared in ClearSee solution (10% xylitol, 15% sodium deoxycholate, 25% urea) either homemade or the commercial formulation from FUJIFILM Wako Pure Chemical Corporation for 2 days at room temperature. Cleared samples were stained with 0.1% Calcofluor-white in ClearSee for 50 min, destained in ClearSee for 15 min, and mounted in ClearSee solution for imaging. For uncut seedling that were used as control: the seedlings were fixated and treated for confocal imaging, but before mounting them on slides for scanning, they were cut to facilitate the scanning, while in cut explants, their leaf petioles were cut before tissue fixation.

Microscopy

Confocal imaging was performed using a Zeiss LSM-02 (800inv_Airyscan) equipped with 10× or 20× dry objectives. Images were acquired at a pixel format of 4096 × 4096, and Z-stacks were collected at 750 × 750. A bidirectional scan was used with a scan speed of 6 and line averaging of 4. Fluorophores were imaged using the following settings: Calcofluor-white (ex. 405 nm; em. 414–471 nm), GFP (ex. 488 nm; em. 491–519 nm), and Venus (ex. 514 nm; em. 518–540 nm). Laser power and pinhole size were adjusted according to fluorescence intensity to avoid signal saturation or photobleaching, and gain was kept at 1. All imaging parameters were maintained constant within all the experiments. Images were processed and analysed using Fiji (ImageJ).

Quantitative Image Analysis and Data Handling

Bright-field images of cultured explant plates were acquired using a flatbed scanner under all experimental conditions (touch, non-touch, and intermediate medium). Root and callus regeneration frequencies were quantified from the scanned plates at each time point (7DAC, 9DAC, 12DAC). Callus surface area (μm^2) was measured using FIJI (https://fiji.sc). Leaf explants were flipped to face the medium at the final time point (the last day of the experiment), then the plates were scanned. Images were converted to 8-bit, thresholds were adjusted, and the Wand (Tracing) tool was used to outline each

callus. The ROI Manager was used to track all calli within each plate and measure their surface areas (µm²). Callus areas of the mutant lines were normalized to the Col-0 mean. Data processing was performed in Excel. Uniform brightness adjustments were applied across all images to enhance visibility while maintaining comparability between treatments.

Statistical Analysis

Data visualization and preliminary organization of the images were performed using Microsoft. Statistical analyses were conducted using GraphPad Prism software. For comparisons between two groups, a two-tailed Student's t-test was applied. When analysing differences among multiple genotypes or treatment conditions at one time point, one-way ANOVA was performed. When analysing differences among multiple genotypes at different time points, a two-way ANOVA analysis was used. All followed by appropriate post hoc tests where applicable. Statistical significance was considered at $p < 0.05$. For the intermediate medium experiments, the figure was obtained from the mean of three independent plates (biological replicas); each replica has 3o explants. Then, one-way ANOVA was used to compare each specific category (DNRR, WICF, WICF+DNRR, No regeneration) among different conditions. This way of analysis was used in the case of intermediate medium, as we care only about the callus category among different conditions.

Author contribution

NK, JF designed the experiments. NK designed and optimized the DNRR and WICF assays and did all other experimental work including quantification and data analysis under the supervision of JF. NK and JF wrote the manuscript.

Acknowledgement

We thank Lukas Fiedler for bringing the idea of working on leaf-derived regeneration to our lab and Lesia Rodriguez for providing the *pTMK4:TMK4-GFP* plasmid. We also gratefully acknowledge Mark Estell, Tongda Xu, Zhenbiao Yang for providing published material. We acknowledge the Scientific Service Units of the Institute of Science and Technology Austria (ISTA), particularly the Imaging and Optics Facility and the Lab Support Facility, for technical support and access to research infrastructure. Research in the Friml laboratory was supported by the European Research Council (ERC; 101142681, CYNIPS), the Austrian Science Fund (FWF; I 6123-B)

Conflicts of Interest

The authors declare no conflicts of interest.

Bibliography

Adamowski M, Matijević I, Friml J. **2024**. Developmental patterning function of GNOM ARF-GEF mediated from the cell periphery. *eLife* **13**.

Aliaga Fandino AC, Hardtke CS. **2022**. Auxin transport in developing protophloem: A case study in canalization. *Journal of Plant Physiology* **269**.

Asai S, Cevik V, Jones JDG, Shirasu K. **2023**. Cell-specific RNA profiling reveals host genes expressed in Arabidopsis cells haustoriated by downy mildew. *Plant Physiology* **193**: 259–270.

Benková E, Michniewicz M, Sauer M, Teichmann T, Seifertová D, Jü Rgens G, Friml J. **2003**. *Local, Efflux-Dependent Auxin Gradients as a Common Module for Plant Organ Formation growing shoots or roots bearing a secondary meristem at the tip. Aerial organs such as leaves and secondary shoots, including flowers, originate from primordia on*.

Birnbaum KD, Alvarado AS. **2008**. Slicing across Kingdoms: Regeneration in Plants and Animals. *Cell* **132**: 697–710.

Bustillo-Avendaño E, Ibáñez S, Sanz O, Barros JAS, Gude I, Perianez-Rodriguez J, Micol JL, del Pozo JC, Moreno-Risueno MA, Pérez-Pérez JM. **2018**. Regulation of hormonal control, cell reprogramming, and patterning during de novo root organogenesis. *Plant Physiology* **176**: 1709–1727.

Cao M, Chen R, Li P, Yu Y, Zheng R, Ge D, Zheng W, Wang X, Gu Y, Gelová Z, *et al.* 2019. TMK1-mediated auxin signalling regulates differential growth of the apical hook. *Nature* **568**: 240–243.

Chen H, Qi L, Zou M, Lu M, Kwiatkowski M, Pei Y, Jaworski K, Friml J. **2025**. TIR1-produced cAMP as a second messenger in transcriptional auxin signalling. *Nature* **640**: 1011–1016.

Chen X, Qu Y, Sheng L, Liu J, Huang H, Xu L. **2014**. A simple method suitable to study de novo root organogenesis. *Frontiers in Plant Science* **5**.

Chu J, Ang ACH, de Roij M, Strader L, Xu T, Weijers D. **2026**. Auxin signaling. *Cell* **189**: 4531–4547.

Duclercq J, Sangwan-Norreel B, Catterou M, Sangwan RS. **2011**. De novo shoot organogenesis: From art to science. *Trends in Plant Science* **16**: 597–606.

Fan M, Xu C, Xu K, Hu Y. **2012**. LATERAL ORGAN BOUNDARIES DOMAIN transcription factors direct callus formation in Arabidopsis regeneration. *Cell Research* **22**: 1169–1180.

Friml J. **2022**. Fourteen Stations of Auxin. *Cold Spring Harbor Perspectives in Biology* **14**.

Friml J, Gallei M, Gelová Z, Johnson A, Mazur E, Monzer A, Rodriguez L, Roosjen M, Verstraeten I, Živanović BD, *et al.* 2022. ABP1–TMK auxin perception for global phosphorylation and auxin canalization. *Nature* **609**: 575–581.

Gao Y, Zhang Y, Zhang D, Dai X, Estelle M, Zhao Y. **2015**. Auxin binding protein 1 (ABP1) is not required for either auxin signaling or Arabidopsis development. *Proceedings of the National Academy of Sciences of the United States of America* **112**: 2275–2280.

Geldner N, Richter S, Vieten A, Marquardt S, Torres-Ruiz RA, Mayer U, Jürgens G. **2004**. Partial loss-of-function alleles reveal a role for GNOM in auxin transport-related, post-embryonic development of Arabidopsis. *Development* **131**: 389–400.

Hajný J, Prát T, Rydza N, Rodriguez L, Tan S, Verstraeten I, Domjan D, Mazur E, Smakowska-Luzan E, Smet W, et al. 2020. Receptor kinase module targets PIN-dependent auxin transport during canalization. *Science* **370(6516): 550–557.**

Hajný J, Tan S, Friml J. **2022**. Auxin canalization: From speculative models toward molecular players. *Current Opinion in Plant Biology* **65**.

Hayashi KI, Neve J, Hirose M, Kuboki A, Shimada Y, Kepinski S, Nozaki H. **2012**. Rational design of an auxin antagonist of the SCF TIR1 auxin receptor complex. *ACS Chemical Biology* **7**: 590–598.

Huang R, Wang J, Chang M, Tang W, Yu Y, Zhang Y, Peng Y, Wang Y, Guo Y, Lu T, *et al.* 2026. Correction to: TMK-PIN1 drives a short self-organizing circuit for auxin export and signaling in Arabidopsis (Developmental Cell, (2025), (S1534580725005696), 10.1016/j.devcel.2025.09.009). *Developmental Cell* **61**: 224–225.

Huang R, Zheng R, He J, Zhou Z, Wang J, Xiong Y, Xu T. **2019**. Noncanonical auxin signaling regulates cell division pattern during lateral root development. *Proceedings of the National Academy of Sciences of the United States of America* **116**: 21285–21290.

Ikeuchi M, Favero DS, Sakamoto Y, Iwase A, Coleman D, Rymen B, Sugimoto K. **2026**. Molecular Mechanisms of Plant Regeneration.

Ikeuchi M, Ogawa Y, Iwase A, Sugimoto K. **2016**. Plant regeneration: Cellular origins and molecular mechanisms. *Development (Cambridge)* **143**: 1442–1451.

Kareem A, van Wüllen AK, Zhang A, Walckiers G, Fasth E, Melnyk CW. **2025**. Water availability positions auxin response maxima to determine plant regeneration fates. *Nature Plants* **11**: 1367–1379.

Klode M, Dahlke RI, Sauter M, Steffens B. **2011**. Expression and Subcellular Localization of Arabidopsis thaliana Auxin-Binding Protein 1 (ABP1). *Journal of Plant Growth Regulation* **30**: 416–424.

Kong S, Zhu M, Roeder AHK. **2025**. Self-organization underlies developmental robustness in plants. *Cells and Development* **184**.

Kuhn A, Roosjen M, Mutte S, Dubey SM, Carrillo Carrasco VP, Boeren S, Monzer A, Koehorst J, Kohchi T, Nishihama R, *et al.* 2024. RAF-like protein kinases mediate a deeply conserved, rapid auxin response. *Cell* **187**: 130-148.e17.

Lavania D, Linh NM, Scarpella E. **2021**. Of cells, strands, and networks: Auxin and the patterned formation of the vascular system. *Cold Spring Harbor Perspectives in Biology* **13**.

Lavy M, Estelle M. **2016**. Mechanisms of auxin signaling. *Development (Cambridge)* **143**: 3226–3229.

Liao CY, Smet W, Brunoud G, Yoshida S, Vernoux T, Weijers D. **2015**. Reporters for sensitive and quantitative measurement of auxin response. *Nature Methods* **12**: 207–210.

Luschnig C, Friml J. **2024**. Over 25 years of decrypting PIN-mediated plant development. *Nature Communications* **15**.

Mazur E, Kulik I, Hajný J, Friml J. **2020**. Auxin canalization and vascular tissue formation by TIR1/AFB-mediated auxin signaling in Arabidopsis. *New Phytologist* **226**: 1375–1383.

Pérez-Henríquez P, Li H, Zhou X, Pan X, Lin W, Tang W, Nagawa S, Lin D, Xu T, Michniewicz M, *et al.* 2024. Hierarchical global and local auxin signals coordinate cellular interdigitation in *Arabidopsis*.

Prigge MJ, Platre M, Kadakia N, Zhang Y, Greenham K, Szutu W, Pandey BK, Bhosale RA, Bennett MJ, Busch W, *et al.* 2020. Genetic analysis of the arabidopsis TIR1/AFB auxin receptors reveals both overlapping and specialized functions. *eLife* **9**.

Qi L, Kwiatkowski M, Chen H, Hoermayer L, Sinclair S, Zou M, del Genio CI, Kubeš MF, Napier R, Jaworski K, *et al.* 2022. Adenylate cyclase activity of TIR1/AFB auxin receptors in plants. *Nature* **611**: 133–138.

Ravichandran SJ, Linh NM, Scarpella E. **2020**. The canalization hypothesis – challenges and alternatives. *New Phytologist* **227**: 1051–1059.

Rodriguez L, Fiedler L, Zou M, Giannini C, Monzer A, Vladimirtsev D, Randuch M, Yu Y, Gelová Z, Verstraeten I, *et al.* 2025. ABP1/ABL3-TMK1 cell-surface auxin signaling targets PIN2-mediated auxin fluxes for root gravitropism. *Cell* **188**: 6138-6150.e17.

Sachs T. **2000**. *Integrating Cellular and Organismic Aspects of Vascular Differentiation*.

Sauer M, Balla J, Luschnig C, Wiśniewska J, Reinöhl V, Friml J, Benková E. **2006**. Canalization of auxin flow by Aux/IAA-ARF-dependent feedback regulation of PIN polarity. *Genes and Development* **20**: 2902–2911.

Sheen J. **2024**. The new horizon of plant auxin signaling via cell-surface co-receptors. *Cell Research* **34**: 343–344.

Sugimoto K, Gordon SP, Meyerowitz EM. **2011**. Regeneration in plants and animals: Dedifferentiation, transdifferentiation, or just differentiation? *Trends in Cell Biology* **21**: 212–218.

Tan S. **2021**. Action mode of NPA: direct inhibition on PIN auxin transporters. *Molecular Plant* **14**: 199.

Vanneste S, Pei Y, Friml J. **2025**. Mechanisms of auxin action in plant growth and development. *Nature Reviews Molecular Cell Biology* **26**: 648–666.

Vieten A, Vanneste S, Wiśniewska J, Benková E, Benjamins R, Beeckman T, Luschnig C, Friml J. **2005**. Functional redundancy of PIN proteins is accompanied by auxin-dependent cross-regulation of PIN expression. *Development* **132**: 4521–4531.

Xu L, Huang H. **2014**. Genetic and Epigenetic Controls of Plant Regeneration. In: Current Topics in Developmental Biology. Academic Press Inc., 1–33.

Yu Y, Tang W, Lin W, Li W, Zhou X, Li Y, Chen R, Zheng R, Qin G, Cao W, *et al.* 2023. ABLs and TMKs are co-receptors for extracellular auxin. *Cell* **186**: 5457-5471.e17.

Zhang J, Mazur E, Balla J, Gallei M, Kalousek P, Medveďová Z, Li Y, Wang Y, Prát T, Vasileva M, *et al.* 2020. Strigolactones inhibit auxin feedback on PIN-dependent auxin transport canalization. *Nature Communications* **11**.

Table S1. List of Arabidopsis mutants and transgenic lines used in this study.

Genotype	Background	Reference
gnom R5	Col-0	*(Geldner et al., 2004)*
tir1	Col-0	*(Prigge et al., 2020)*
tir1;afb2;afb3	Col-0	*(Prigge et al., 2020)*
XVE>>axr3-mCherry	Col-0	(Chen *et al.*, 2025)
XVE>>axr3-mCherry-KUP5	Col-0	(Chen *et al.*, 2025)
XVE>>axr3-mCherry-KUP5m	Col-0	(Chen *et al.*, 2025)
pABP1:GUS	Col-0	*(Klode et al., 2011)*
pABL3:GUS	Col-0	*(Asai et al., 2023)*
pTMK1:GUS	Col-0	*(Friml et al., 2022)*
pTMK3:GUS	Col-0	*(Friml et al., 2022)*
pTMK4:GUS	Col-0	*(Friml et al., 2022)*
TMK1:gTMK1-GFP;tmk1-1	Col-0	*(Rodriguez et al., 2025)*
pDR5:nVenus	Col-0	*(Liao et al., 2015)*
pPIN3:GUS	Col-0	*(Friml et al., 2002)*
pPIN4:GUS	Col-0	*(Benková et al., 2003)*
pPIN7:GUS	Col-0	*(Vieten et al., 2005)*
pin1-1	Col-0	*(Vieten et al., 2005)*
pPIN1:PIN1-GFP	Col-0	*(Benková et al., 2003)*
tmk1-1	Col-0	*(Cao et al., 2019)*
tmk1;2;3	Col-0	*(Cao et al., 2019)*
tmk4	Col-0	*(Cao et al., 2019)*
abp1-C1	Col-0	*(Gao et al., 2015)*
abp1-TD1	Col-0	*(Gao et al., 2015)*
abp1-TD1;abl1;abl2	Col-0	*(Yu et al., 2023)*

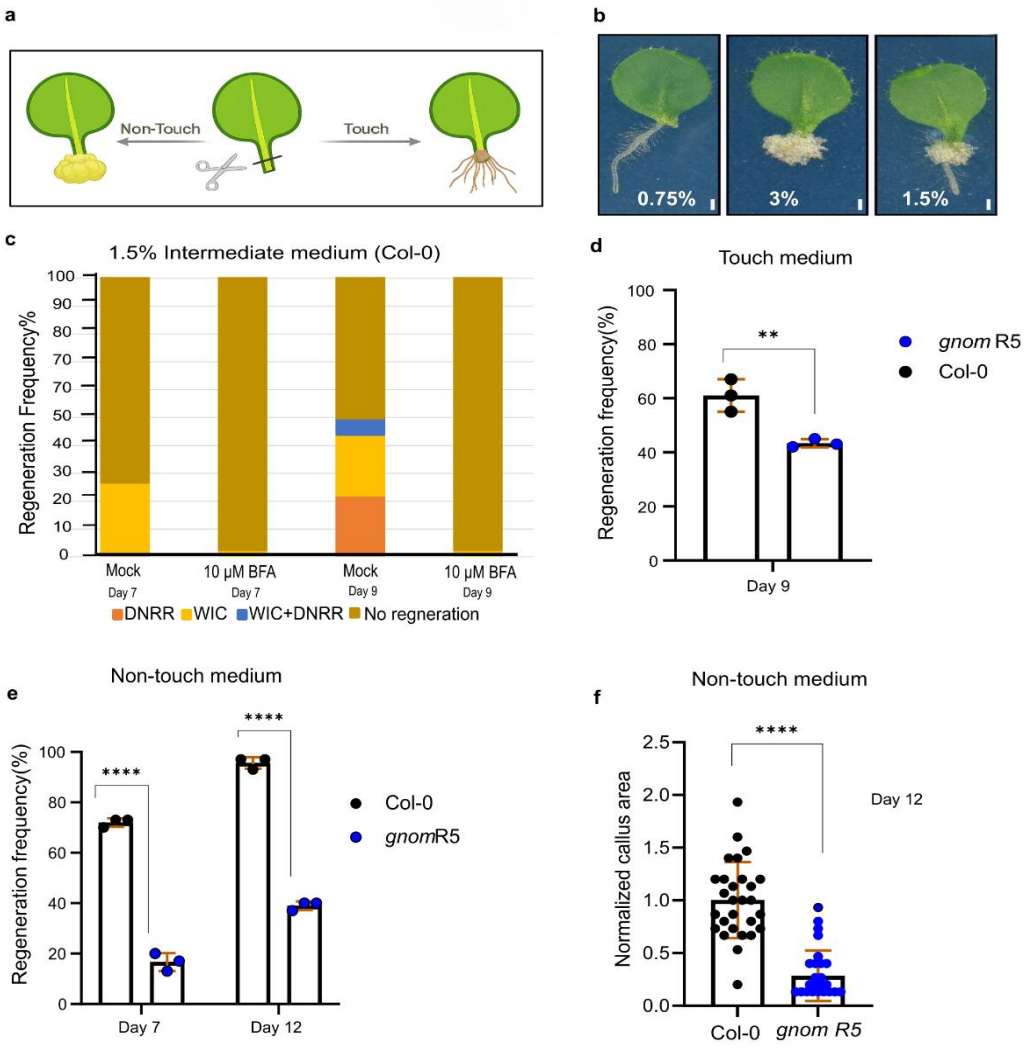

772

773

774 **Fig. 1| PIN-dependent auxin transport and PIN trafficking in leaf-derived**
775 **regeneration.**

776 **a,** Schematic of different regeneration modes under non-touch (callus formation; WICF) and
777 touch (root formation; DNRR) conditions. **b,** Regeneration at different agar concentrations:
778 0.75% supports DNRR; 3% or flipped explants form WICF; 1.5% leads to callus formation
779 followed by root emergence after 1-2 days. Scale bar, 500 µm. **c,** Regeneration frequency after
780 treatment with PIN trafficking inhibitor BFA (10 µM) in intermediate medium (1.5%) (n = 90
781 explants; mean of three plates of 30 explants each; two-tailed Student's t-test). **d,** Regeneration
782 frequency in the *gnom R5* mutant in touch medium (0.75%) at day 9 (n = 90 explants per
783 genotype; mean of three plates; **P < 0.01, Student's t-test). **e** and **f,** Regeneration frequency in
784 *gnom R5* in non-touch medium at days 7 and 12 (e). Normalized callus area (n = 50-60
785 independent explants) (f) (****P < 0.0001; two-tailed Student's t-test). In **c**, **d**, **e** and **f**, three
786 independent experiments produced identical results.

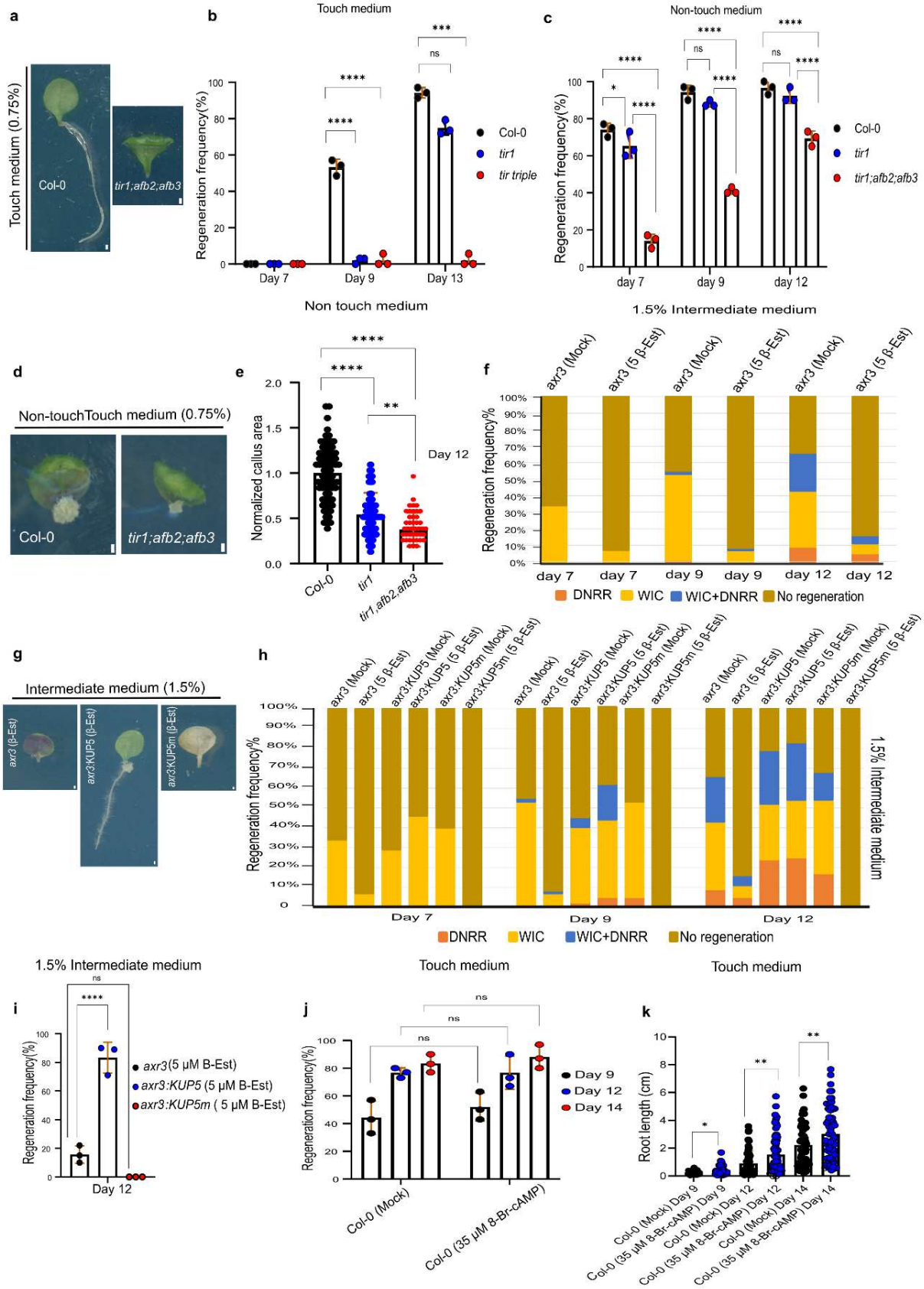
a
Touch medium (0.75%)
Col-0
tir1;afb2;afb3
b
Touch medium
Regeneration frequency(%)
Day 7
Day 9
Day 13
Col-0
tir1
tir triple
c
Non-touch medium
Regeneration frequency(%)
day 7
day 9
day 12
Col-0
tir1
tir1;afb2;afb3
Non touch medium
1.5% Intermediate medium
d
Non-touchTouch medium (0.75%)
Col-0
tir1;afb2;afb3
e
Normalized callus area
Day 12
Col-0
tir1
tir1,afb2,afb3
f
Regeneration frequency%
axr3 (Mock)
axr3 (5 β-Est)
DNRR
WIC
WIC+DNRR
No regeneration
g
Intermediate medium (1.5%)
axr3 (β-Est)
axr3:KUP5 (β-Est)
axr3:KUP5m (β-Est)
h
Regeneration frequency%
axr3:KUP5 (Mock)
axr3:KUP5 (5 β-Est)
axr3:KUP5m (Mock)
axr3:KUP5m (5 β-Est)
Day 7
Day 9
Day 12
1.5% Intermediate medium
DNRR
WIC
WIC+DNRR
No regeneration
1.5% Intermediate medium
i
Regeneration frequency(%)
axr3(5 μM B-Est)
axr3:KUP5 (5 μM B-Est)
axr3:KUP5m (5 μM B-Est)
Day 12
Touch medium
j
Regeneration frequency(%)
Day 9
Day 12
Day 14
Col-0 (Mock)
Col-0 (35 μM 8-Br-cAMP)
Touch medium
k
Root length (cm)
Col-0 (Mock) Day 9
Col-0 (35 μM 8-Br-cAMP) Day 9
Col-0 (Mock) Day 12
Col-0 (35 μM 8-Br-cAMP) Day 12
Col-0 (Mock) Day 14
Col-0 (35 μM 8-Br-cAMP) Day 14

Fig. 2 | TIR1/AFB-mediated nuclear auxin signalling in leaf-derived regeneration.

a, Representative images showing DNRR in Col-0 and *tir1;afb2;afb3* under touch conditions. Scale bar, 500 µm. **b** and **c,** Regeneration frequencies of Col-0, *tir1*, and *tir1;afb2;afb3* under touch (b) and non-touch (c) conditions (n = 90 explants per genotype; mean of three plates; for touch, ****P < 0.0001 at day 9, for non-touch, *P < 0.05, ****P < 0.0001 at day 7; two-factor ANOVA). **d,** Representative images showing WICF in Col-0 and *tir1;afb2;afb3* under non-touch conditions. Scale bar, 500 µm. **e,** Normalized callus area (WICF) in *tir1* and *tir1;afb2;afb3* at day 12 (n = 50–60 explants; ****P < 0.0001, ****P < 0.0001; One-factor ANOVA). **f,** Regeneration frequency of *XVE≫axr3:mCherry* estradiol-inducible line under intermediate medium (1.5%) at days 7, 9, and 12 using 5 µM β-Est (n = 90 explants per genotype; mean of three plates). **g,** Representative images of *XVE≫axr3:mCherry*, *XVE≫axr3-KUP5:mCherry* (axr3 fused with cAMP producing KUP5 enzyme), and *XVE≫axr3-KUP5m:mCherry* (control, mutated KUP5) treated with β-Est, supplemented to intermediate medium. Scale bar, 500 µm. **h,** Regeneration frequencies of *axr3*, *axr3*:KUP5, and *axr3*:mKUP5 in intermediate medium (5 µM β-Est) (n = 90 explants per genotype; mean of three plates). **i**, Total regeneration frequencies of *axr3*, *axr3*-KUP5 and *ax3*-KUP5m under 5 µM β-Est at day 12; data is summarized from Fig. 2h. **j,** Regeneration frequencies of Col-0 under touch medium in mock and 35 µM 8-Br-cAMP treatments (n = 90 explants per genotype; mean of three plates; two-way ANOVA; ns). **k,** Root length (cm) of Col-0 treated or untreated with 35 µM 8-Br-cAMP under touch medium (n = 50-60 explants) (Student's t-test; *P < 0.05, **P < 0.01, **P < 0.01). In **b**, **c**, **e**, **f**, **h**, **i**, and **j**, three independent experiments produced identical results.

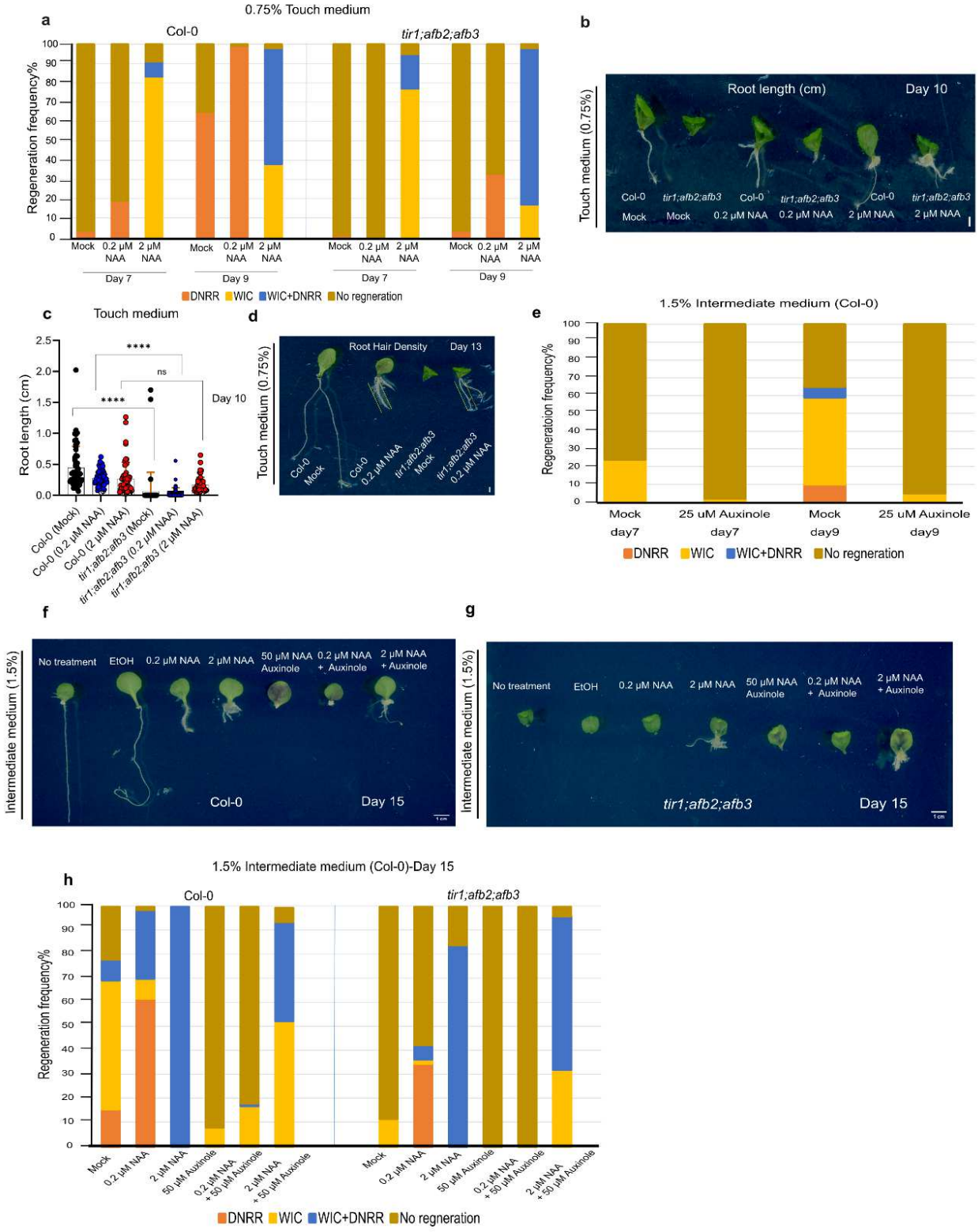
a
0.75% Touch medium
Col-0
tir1;afb2;afb3
Regeneration frequency%
Mock
0.2 μM NAA
2 μM NAA
Day 7
Day 9
DNRR
WIC
WIC+DNRR
No regneration
b
Root length (cm)
Day 10
Touch medium (0.75%)
Col-0
tir1;afb2;afb3
Mock
0.2 μM NAA
2 μM NAA
c
Touch medium
Root length (cm)
Day 10
****
ns
Col-0 (Mock)
Col-0 (0.2 μM NAA)
Col-0 (2 μM NAA)
tir1;afb2;afb3 (Mock)
tir1;afb2;afb3 (0.2 μM NAA)
tir1;afb2;afb3 (2 μM NAA)
d
Root Hair Density
Day 13
Touch medium (0.75%)
e
1.5% Intermediate medium (Col-0)
Regeneratoion frequency%
Mock
25 uM Auxinole
day7
day9
DNRR
WIC
WIC+DNRR
No regneration
f
Intermediate medium (1.5%)
No treatment
EtOH
0.2 μM NAA
2 μM NAA
50 μM NAA Auxinole
0.2 μM NAA + Auxinole
2 μM NAA + Auxinole
Col-0
Day 15
g
tir1;afb2;afb3
h
1.5% Intermediate medium (Col-0)-Day 15
Col-0
tir1;afb2;afb3
Regeneration frequency%
Mock
0.2 μM NAA
2 μM NAA
50 μM Auxinole
0.2 μM NAA + 50 μM Auxinole
2 μM NAA + 50 μM Auxinole
DNRR
WIC
WIC+DNRR
No regneration

Fig. 3 | Exogenous auxin-induced rescues of the TIR1/AFB deficiency in leaf-derived regeneration.

a, Regeneration frequencies of Col-0 and *tir1;afb2;afb3* treated with NAA (0.2 µM and 2 µM) in touch conditions (n = 90 explants per genotype; 30 explants per plate; mean of three plates). **b,** Representative images showing root length (cm) of Col-0 and *tir1;afb2;afb3* treated with NAA (0.2 µM and 2 µM) at day 10 in touch conditions. Scale bar, 0.5 cm. **c,** Root length quantification (cm) of (b) (50-60 roots were used). **d,** Representative images showing root hair density of Col-0 and *tir1;afb2;afb3* treated with NAA (0.2 µM) at day 13 under touch conditions. Scale bar, 0.5 cm. **e,** Regeneration frequency of Col-0 treated with 50 µM Auxinole in intermediate medium (n = 90 explants; three plates of 30 explants each). **f** and **g,** Representative images of Col-0 (f) or *tir1;afb2;afb3* (g) explants treated with 0.2 µM NAA, 2 µM NAA, 50 µM Auxinole, 0.2 µM NAA + 50 µM Auxinole, and 2 µM NAA + 50 µM Auxinole in intermediate medium at day 15. Scale bar, 1 cm. **h,** Regeneration frequencies of Col-0 and *tir1;afb2;afb3* co-treated with 0.2 µM NAA + 50 µM Auxinole or 2 µM NAA + 50 µM Auxinole, compared with controls (mock, 0.2 µM NAA, 2 µM NAA, 50 µM Auxinole) in intermediate medium at day 15 (n = 90 explants; three plates of 30 explants each; mean). In **a**, **c**, **e** and **h**, three independent experiments produced identical results.

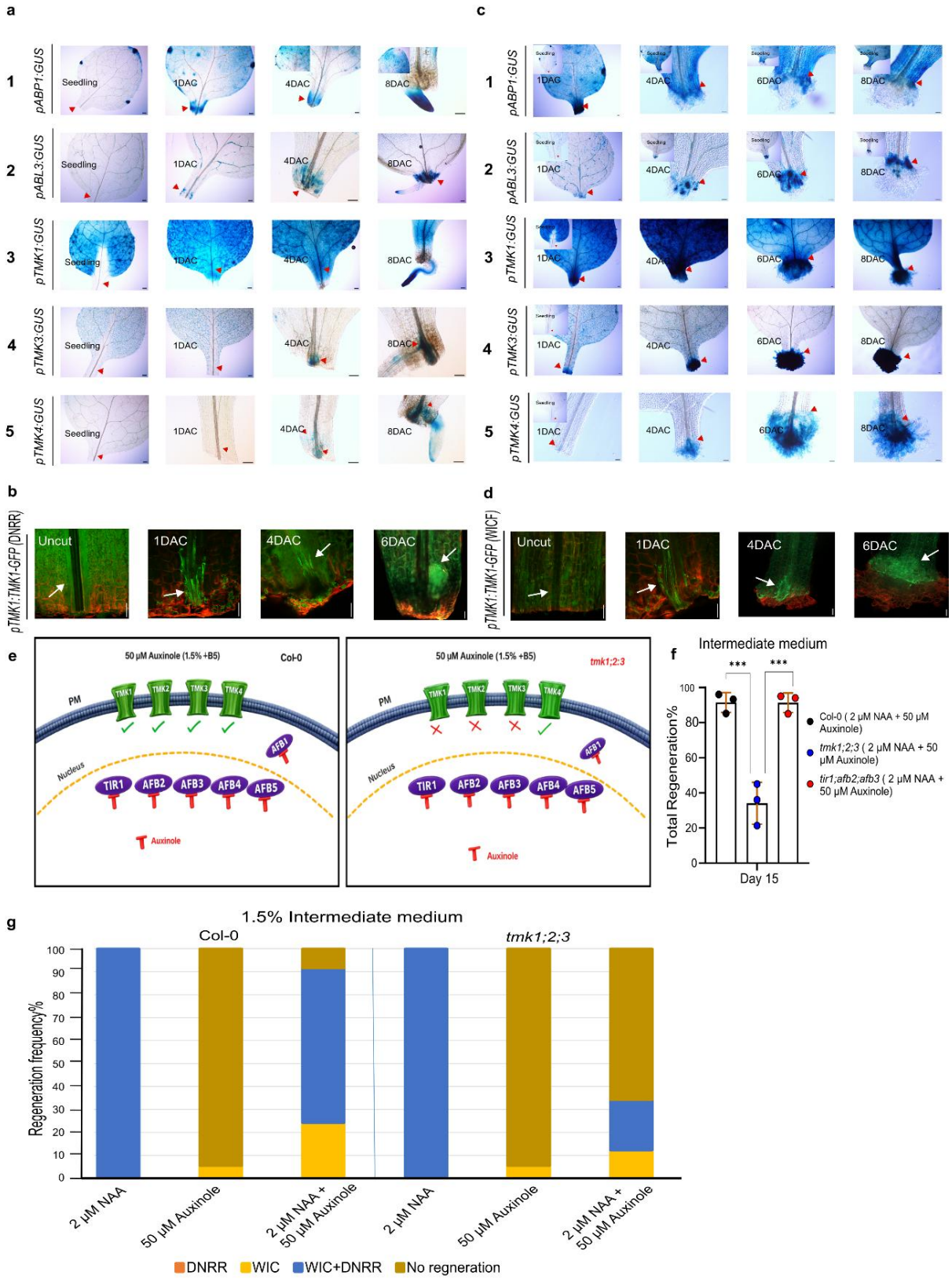
a
1
pABP1:GUS
Seedling
1DAC
4DAC
8DAC
2
pABL3:GUS
3
pTMK1:GUS
4
pTMK3:GUS
5
pTMK4:GUS
c
6DAC
b
pTMK1:TMK1-GFP (DNRR)
Uncut
d
pTMK1:TMK1-GFP (WICF)
e
50 μM Auxinole (1.5% +B5)
Col-0
tmk1;2;3
PM
TMK1
TMK2
TMK3
TMK4
Nucleus
TIR1
AFB1
AFB2
AFB3
AFB4
AFB5
Auxinole
f
Intermediate medium
***
Total Regeneration%
Day 15
Col-0 (2 μM NAA + 50 μM Auxinole)
tmk1;2;3 (2 μM NAA + 50 μM Auxinole)
tir1;afb2;afb3 (2 μM NAA + 50 μM Auxinole)
g
1.5% Intermediate medium
Regeneration frequency%
2 μM NAA
50 μM Auxinole
2 μM NAA + 50 μM Auxinole
DNRR
WIC
WIC+DNRR
No regneration

Fig. 4 | ABP1–TMK cell-surface auxin perception in leaf-derived regeneration.

a and **c,** Time course of ABP1, ABL3, TMK1, TMK3, and TMK4 expression during DNRR (a) or WICF (c) using *promotor::GUS* lines under touch (a) or non-touch (c) conditions as compared to uncut Arabidopsis seedlings. Scale bar, 100 µm. **b** and **d,** TMK1 localization from *TMK1:TMK1-GFP* (green) in DNRR under touch (b) and in WICF under non-touch conditions (d) as compared to uncut seedlings. Minimum of 10 explants were scanned per time point; three independent experiments showed identical patterns. The white arrows indicate the expression pattern of the TMK1 at the wound area during DNRR and WICF. Scale bar, 50 µm. **e,** Schematics illustrating the strategy used to manipulate TIR1/AFB and ABP1/ABL-TMK signalling. **f**, Total regeneration frequencies of Col-0, *tmk1;2;3*, and *tir1;afb2;afb3* co-treated with 2 µM NAA + 50 µM Auxinole in intermediate medium (n = 90 explants per genotype; 30 explants per plate; mean of three plates). Three independent experiments produced identical results. **g,** Detailed regeneration frequencies of Col-0 and *tmk1;2;3* co-treated with NAA and Auxinole. In confocal experiments **b** and **d**, Calcofluor-white (red) was used to stain cell walls. In GUS staining experiments **a**, **c**: more than 10 explants were scanned per time point; three independent experiments showed identical patterns. The red arrowheads indicate the expression of the gene at the wound area.

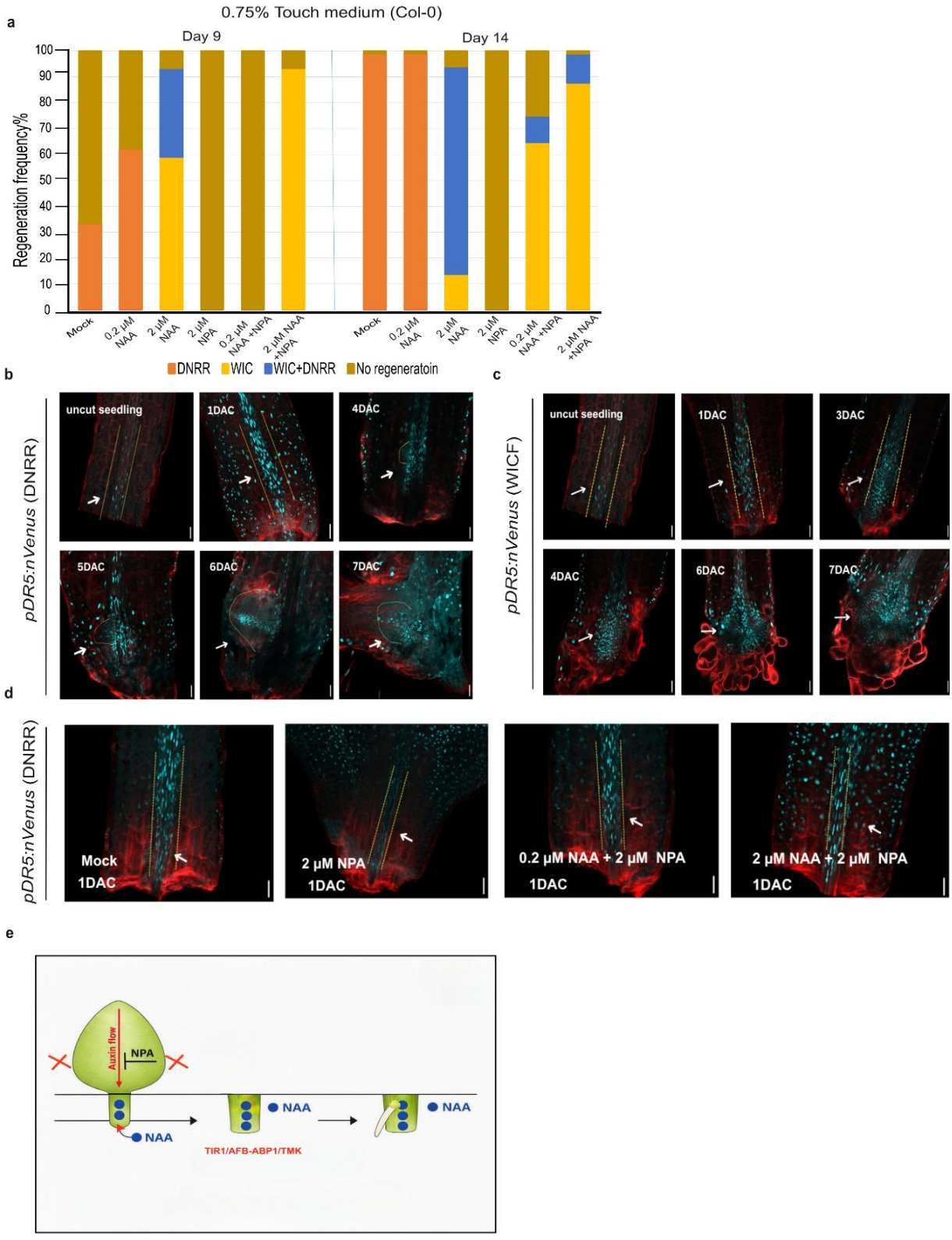
a
0.75% Touch medium (Col-0)
Day 9
Day 14
Regeneration frequency%
100
90
80
70
60
50
40
30
20
10
0
Mock
0.2 μM NAA
2 μM NAA
2 μM NPA
0.2 μM NAA +NPA
2 μM NAA +NPA
DNRR
WIC
WIC+DNRR
No regeneratoin
b
pDR5:nVenus (DNRR)
uncut seedling
1DAC
4DAC
5DAC
6DAC
7DAC
c
pDR5:nVenus (WICF)
uncut seedling
1DAC
3DAC
4DAC
6DAC
7DAC
d
pDR5:nVenus (DNRR)
Mock
1DAC
2 μM NPA
1DAC
0.2 μM NAA + 2 μM NPA
1DAC
2 μM NAA + 2 μM NPA
1DAC
e
Auxin flow
NPA
NAA
NAA
NAA
TIR1/AFB-ABP1/TMK

848

849

Fig. 5| TIR1/AFB and PIN-mediated auxin delivery to the regeneration site.

a, Regeneration frequency of Col-0 explants co-treated with 0.2 µM NAA + 2 µM NPA or 2 µM NAA + 2 µM NPA compared with controls (Mock, 0.2 µM NAA, 2 µM NAA, 2 µM NPA) on intermediate medium (n = 90 explants; 30 per plate; mean of three plates; three independent experiments). **b**, Time course of *pDR5:nVenus* (Triquase colour) during DNRR under touch conditions as compared with uncut seedlings; Scale bar, 50 µm. **c**, Time course of *pDR5:nVenus* (Triquase) during WICF under non-touch conditions as compared to uncut seedlings; Scale bar, 50 µm. **d**, *pDR5:nVenus* (Triquase) during DNRR at 1 DAC under touch conditions following treatment with 2 µM NAA + 2 µM NPA compared with controls (Mock, 2 µM NPA); Scale bar, 50 µm. **e**, Schematic illustrating the experimental setup in which leaf explants are treated with NPA and NAA (2 µM NAA) under touch conditions. In confocal microscope experiments **b**, **c, d**; dashed yellow lines mark petiole vasculature and white arrows indicate long-distance auxin transport and distal auxin maxima specifying root primordium formation and root emergence in **b** or proximal auxin maxima initiating callus formation in **c** or highlighting nuclear auxin signalling-dependent long-distance auxin transport in **d** (≥10 explants per time point; three independent experiments).

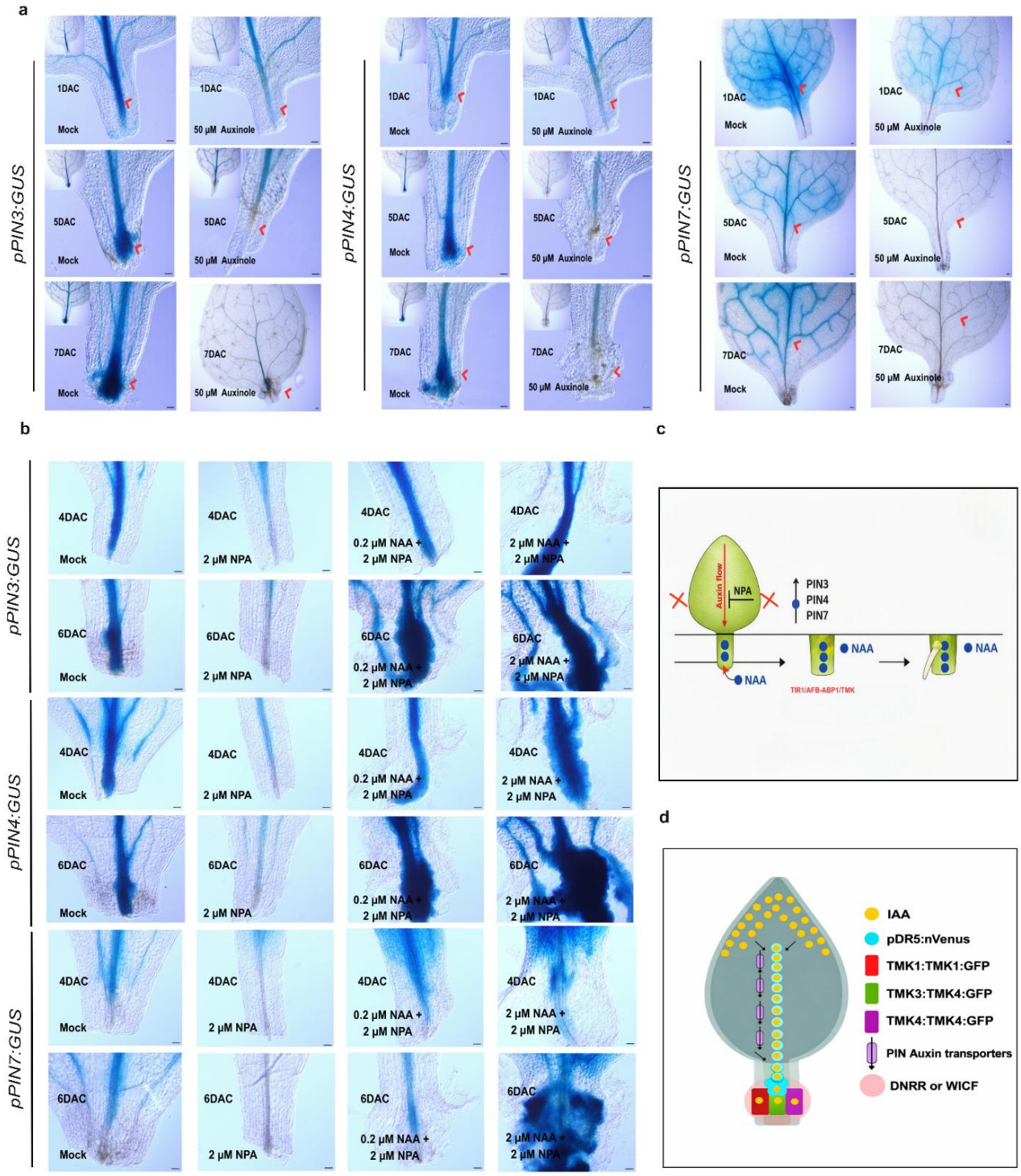
a
pPIN3:GUS
pPIN4:GUS
pPIN7:GUS
1DAC
5DAC
7DAC
Mock
50 μM Auxinole
b
4DAC
6DAC
2 μM NPA
0.2 μM NAA + 2 μM NPA
2 μM NAA + 2 μM NPA
c
Auxin flow
NPA
PIN3
PIN4
PIN7
NAA
TIR1/AFB-ABP1/TMK
d
IAA
pDR5:nVenus
TMK1:TMK1:GFP
TMK3:TMK4:GFP
TMK4:TMK4:GFP
PIN Auxin transporters
DNRR or WICF

Fig. 6| TIR1/AFB auxin signalling controlling PIN expression for auxin supply and downstream ABP1–TMK signalling at the regeneration site.

a and **b,** Time course of PIN3, PIN4 and PIN7 expression using *promotor::GUS* lines in intermediate medium supplemented with either 50 µM Auxinole (a) or 2 µM NPA, 0.2 µM NAA + 2 µM NPA, or 2 µM NAA + 2 µM NPA (b) as compared to the untreated leaf explants (Mock). Red arrowheads indicate the PIN expression at the proliferative cells in the wound area. More than 10 explants were scanned per time point; three independent experiments showed identical patterns. Scale bar, 100 µm. **c,** Schematic illustrating the experimental setup in which *pPIN3/4/7:GUS* leaf explants are treated with NPA and NAA under touch conditions to assess PIN transcriptional induction under blocked auxin transport in response to exogenous NAA supplementation. **d**, Integrative model showing how TIR1/AFB nuclear auxin signalling controls wound-induced PIN-dependent auxin transport from the leaf blade to the wound area (Auxin canalization) while wound-induced ABP1/ABL-TMK together with TIR1/AFB interprets the endogenously delivered or exogenously supplied auxin at the wound area to mediate regeneration (either DNRR or WICF).

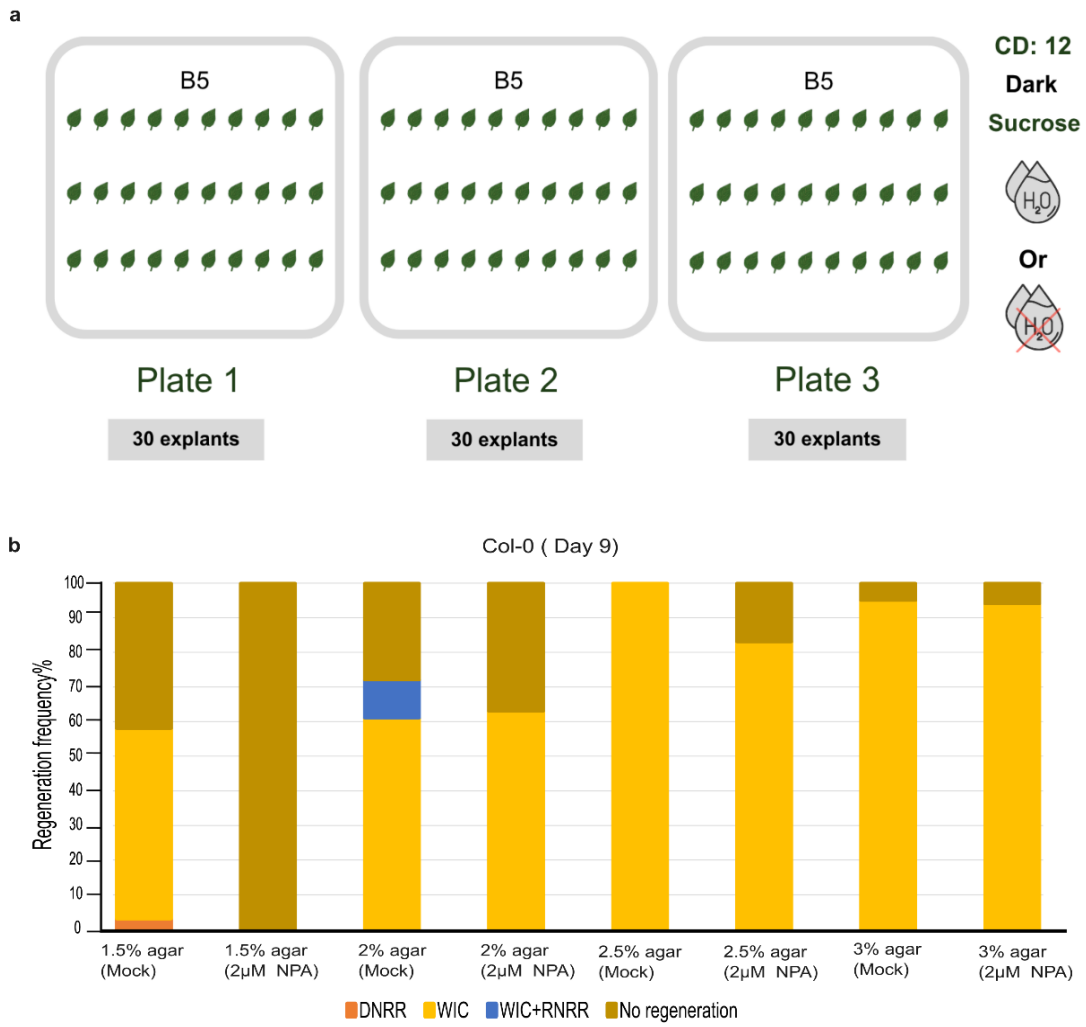

Fig. S1| Optimization of *de novo* root regeneration (DNRR) and Wound-induced callus formation (WICF) assays.

a, Optimized experimental setup for DNRR and WICF assays. Three independent plates (30 leaf explants each) were always cultured in darkness with sucrose under high- or low-water conditions. Cutting day (CD) is day 12. Regeneration frequency (% of formed root or callus) was quantified per plate. **b,** Regeneration frequency of Col-0 treated with 2 µM NPA compared to untreated cut explants at mediums with different agar concentrations (1,5%, 2%, 2.5% and 3%) at day 9; n = 90 explants; 30 per plate; mean of three plates; three independent experiments).

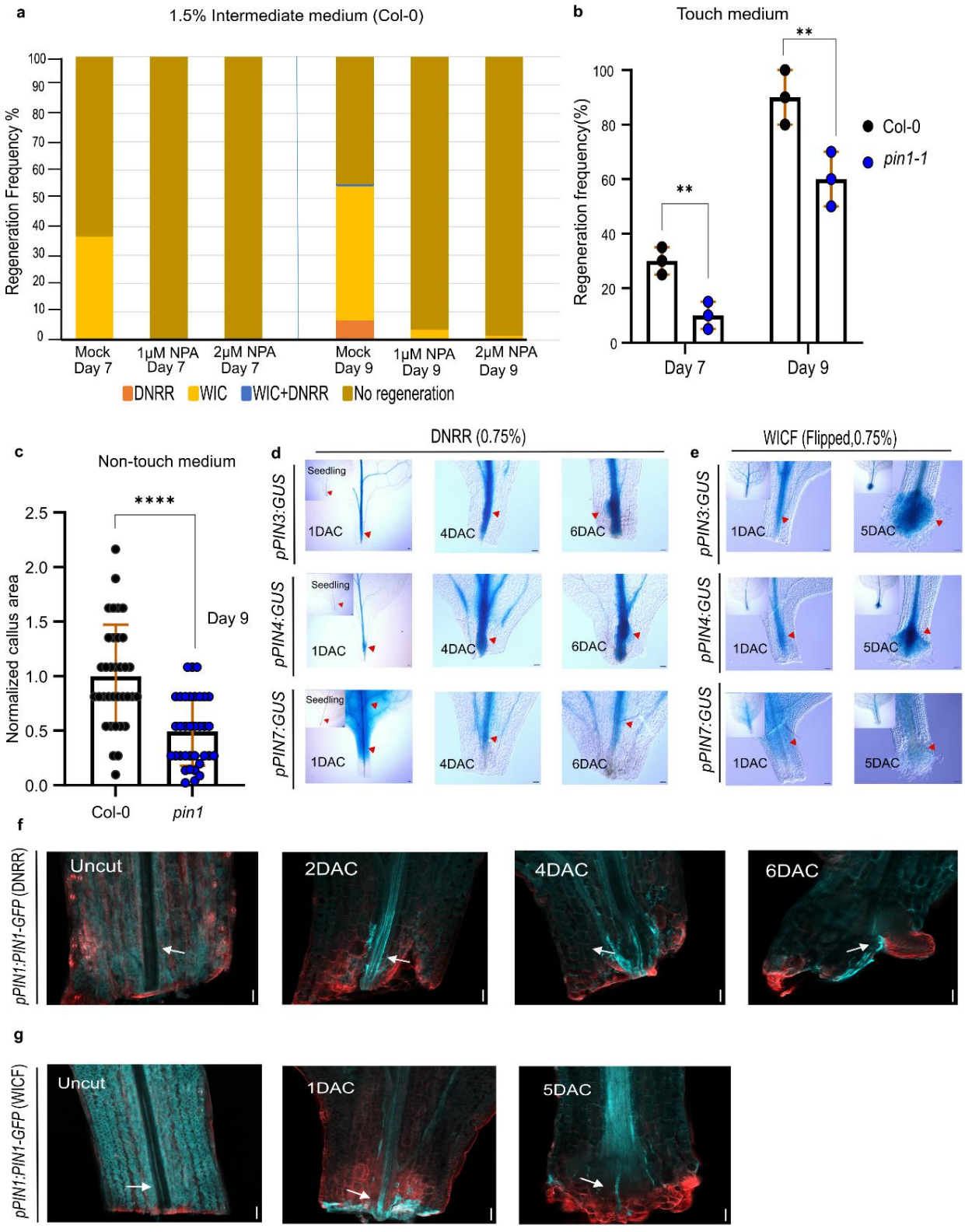
a
1.5% Intermediate medium (Col-0)
Regeneration Frequency %
Mock Day 7
1μM NPA Day 7
2μM NPA Day 7
Mock Day 9
1μM NPA Day 9
2μM NPA Day 9
DNRR
WIC
WIC+DNRR
No regeneration
b
Touch medium
Regeneration frequency(%)
Col-0
pin1-1
Day 7
Day 9
c
Non-touch medium
Normalized callus area
Day 9
Col-0
pin1
d
DNRR (0.75%)
e
WICF (Flipped,0.75%)
pPIN3:GUS
pPIN4:GUS
pPIN7:GUS
Seedling
1DAC
4DAC
5DAC
6DAC
f
pPIN1:PIN1-GFP (DNRR)
Uncut
2DAC
4DAC
6DAC
g
pPIN1:PIN1-GFP (WICF)
Uncut
1DAC
5DAC

Fig. S2| **PIN-dependent long-distance auxin transport in leaf derived regeneration.**

a, Regeneration frequency of Col-0 treated with NPA (1 µM, 2 µM) as compared to the untreated explants in intermediate medium (n = 90 explants; 30 per plate; mean of three plates). **b**, Regeneration frequencies of Col-0 and *pin1-1* heterozygous line under touch conditions (n= 90 explants; 30 per plate; mean of three plates. **P < 0.01, day 7; two-tailed Student's t-test). **c**, Normalized callus area (WICF) in *pin1-1* heterozygous line compared to Col-0 (n = 50-60 independent explants per genotype; ****P < 0.0001, day 9; two-tailed Student's t-test). In **a**, **b**, and **c**, three independent experiments produced identical results. **d** and **e,** Time course of PIN3, PIN4 and PIN7 expression during DNRR (d) or WICF (e) using *promotor::GUS* lines under touch (d) or non-touch (e) conditions. More than 10 explants were scanned per time point; three independent experiments showed identical patterns. The red arrows indicate PINs expression at the wound area in response to leaf petiole wounding. Scale bar, 100 µm. **f** and **g,** Time course of *pPIN1:PIN1-GFP* (Triquase) expression in DNRR under touch conditions (f) or in WICF under non-touch conditions as compared to uncut seedlings (g). More than 10 explants were scanned per time point; three independent experiments showed identical patterns. Scale bar, 50 µm.

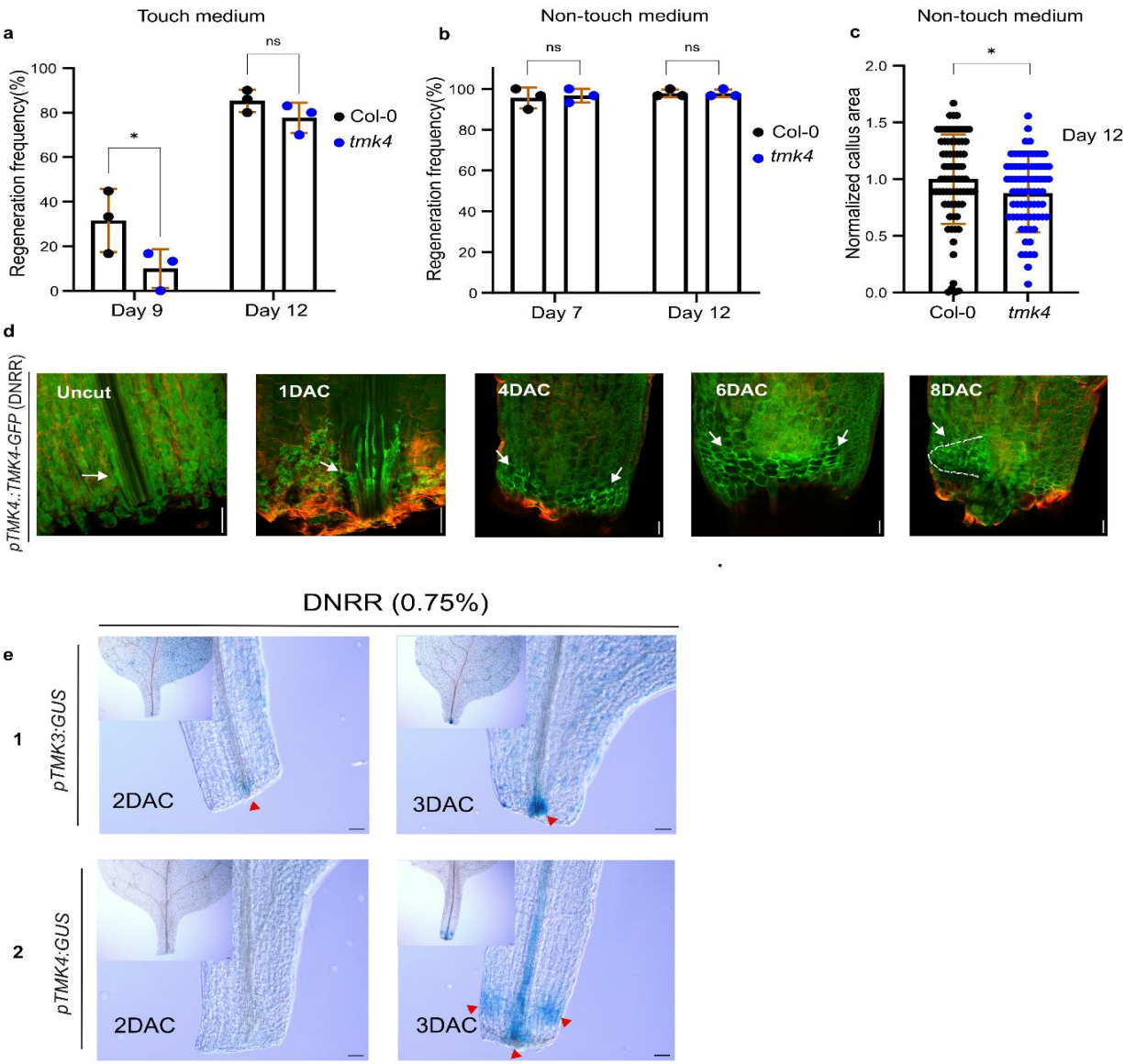

Fig. S3| TMK4 in leaf-derived regeneration.

a and **b,** Regeneration frequencies of Col-0 and *tmk4* in touch (a) and non-touch (b) conditions (n= 90 explants; 30 per plate; mean of three plates. *P < 0.05, day 9; ns, day 12; two-factor ANOVA). **c**, Normalized callus area (WICF) in *tmk4* compared to Col-0 (n = 50-60 independent explants per genotype; *P < 0.05, day 12; two-tailed Student's t-test). In **a**, **b**, and **c**, two independent experiments produced identical results. **d**, Time course of *pTMK4:TMK4-GFP* expression (green) in DNRR under touch conditions as compared to uncut seedlings. More than 10 explants were scanned per time point; three independent experiments showed identical patterns. Scale bar, 50 µm. **e**, Time course of TMK3 (1), and TMK4 (2) expression during DNRR under touch conditions using GUS reporters. Scale bar, 100 µm.



933

934 **Fig. S4| Auxin induction of PIN expression during leaf-derived regeneration under**
935 **both normal or blocked long-distance auxin transport**

936 **a-c,** Expression patterns of *pPIN3:GUS* (a), *pPIN4:GUS* and *pPIN7:GUS* during DNRR
937 co-treated with 0.2 µM NAA + 2 µM NPA or 2 µM NAA + 2 µM NPA as compared to the
938 controls (Mock, 0,2 µM NAA, 2 µM NAA, 2 µM NPA) under touch conditions. More than
939 10 explants were scanned per time point; three independent experiments showed
940 identical patterns. Scale bar, 100 µm.

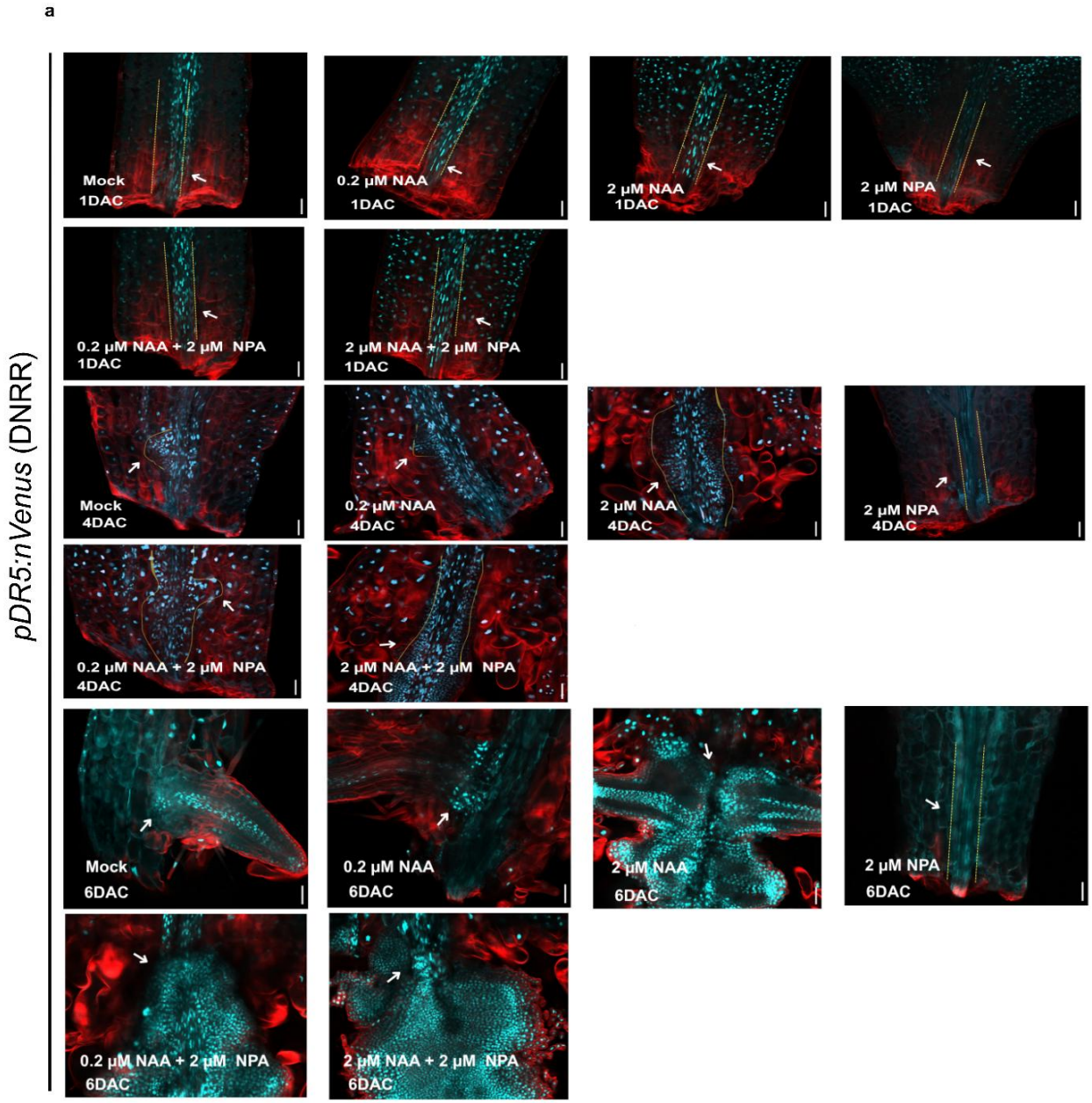

941

942 **Fig. S5| Visualization of nuclear auxin response under conditions of inhibited**
943 **auxin transport and exogenous auxin supplementation.**

944 **a**, Time course of *pDR5:nVenus* auxin response (Triquase) during DNRR under touch
945 conditions following treatment with 0.2 µM NAA + 2 µM NPA or 2 µM NAA + 2 µM NPA
946 as compared with controls (Mock, 0.2 µM NAA, 2 µM NAA, 2 µM NPA), dashed yellow
947 lines mark petiole vasculature and white arrows indicate long-distance auxin transport
948 and distal auxin maxima specifying root primordium formation and emergence (≥10
949 explants per time point; three independent experiments; Scale bar, 50 µm).